DISSERTATIONS IN
FORESTRY AND
NATURAL SCIENCES

Jukka Antikainen

New Techniques for Spectral Image Acquisition and Analysis

Publications of the University of Eastern Finland
Dissertations in Forestry and Natural Sciences No 73

UNIVERSITY OF
EASTERN FINLAND

JUKKA ANTIKAINEN

New Techniques for Spectral Image Acquisition and Analysis

Publications of the University of Eastern Finland
Dissertations in Forestry and Natural Sciences
No 73

Academic Dissertation
To be presented by permission of the Faculty of Science and Forestry for public examination in the Auditorium Louhela at the Joensuu Science Park, Joensuu, on June 15, 2012,
at 12:00 noon.

School of Computing

Kopijyvä Oy
Joensuu, 2012
Editor: Profs. Pertti Pasanen and Pekka Kilpeläinen

Distribution:
University of Eastern Finland Library / Sales of publications
P.O. Box 107, FI-80101 Joensuu, Finland
tel. +358-50-3058396
http://www.uef.fi/kirjasto

ISBN: 978-952-61-0817-9 (printed)
ISSNL: 1798-5668
ISSN: 1798-5668
ISBN: 978-952-61-0818-6 (pdf)
ISSNL: 1798-5668
ISSN: 1798-5676

Author's address:
Finnish Forest Research Institute
Joensuu Unit
P.O.Box 68
80101 JOENSUU
FINLAND
email: jukka.antikainen@metla.fi

Supervisors:
Professor Markku Hauta-Kasari, Ph.D.
University of Eastern Finland
School of Computing
P.O.Box 111
80101 JOENSUU
FINLAND
email: markku.hauta-kasari@uef.fi

Professor Timo Jääskeläinen, Ph.D.
University of Eastern Finland
Department of Physics and Mathematics
P.O.Box 111
80101 JOENSUU
FINLAND
email: timo.jaaskelainen@uef.fi

Reviewers:
Professor Jon Hardeberg, Ph.D.
Gjøvik University College
The Norwegian Color Research Laboratory
P.O.Box 191
N-2818 Gjøvik
NORWAY
email: jon.hardeberg@hig.no

Professor Janne Heikkilä, Dr. Tech.
University of Oulu
Department of Computer Science and Engineering
P.O.Box 4500
FIN-90014 Oulu
FINLAND
email: janne.heikkila@ee.oulu.fi

Opponent:
Professor Heikki Kälviäinen, Dr. Tech.
Lappeenranta University of Technology
Department of Information Technology
P.O.Box 20
FIN-53851 Lappeenranta
FINLAND
email: heikki.kalviainen@lut.fi

ABSTRACT

This thesis describes typical spectral imaging techniques and spectral image analysis algorithms that are in general use. Three developed spectral imaging systems are proposed.

The first imaging system consists of two line scanning based spectral cameras. These cameras are combined in one simultaneous measuring process, which can be used for capturing a wide range of spectral information that cannot be obtained by a single sensor system. The second imaging system is proposed for heartwood detection in Scots Pine (*Pinus sylvestris*). The detection is done using fluorescence and this work proposes a prototype system for online measurements using fluorescence imaging. The third spectral imaging system is proposed for medical applications. This system is small and lightweight and has been connected to a medical microscope and used for neurosurgical operations. The system was also used to collect a database of biological tissues and the resulting images have been tested for correct identification of healthy and neoplastic tissues.

This thesis proposes the implementation of two statistical methods for spectral image analysis. Implementations are done using Graphical Processing Units (GPUs) and computational speed-up of the analyzing algorithms was compared against ordinary (non-GPU) implementations. The first implementation used Principal Component Analysis (PCA), which produced about $7\times$ speed-up for the total computational efficiency. The second implementation used Non-negative Tensor Factorization (NTF), which produced a $60 - 100\times$ speed-up for the total computational efficiency. The imaging systems and software implementations have been used in research projects that are presented as case studies in the thesis.

Universal Decimal Classification: 535.33, 535.651, 778.3
PACS Classification: 02.70.Hm, 07.05.Pj, 42.30.-d, 42.30.Va
Keywords: spectra; color; imaging; spectral analysis; image scanners; cameras; fluorescence; wood; medical image processing; biological tissues; statistical analysis; principal component analysis; tensors

Preface

Around six years ago, when I was planning to move to Joensuu, one of my Master's thesis supervisors at the University of Kuopio said to me "Are you interested in studying colors? There is a really good color research group at Joensuu". At that time, I had no clue what color research actually entailed. During the past six years I have realized how useful and diversified the field of color research actually is. My thanks to Professor Markku Hauta-Kasari who gave me an opportunity to work in the color research group. I would also like to give thanks to him for supervising me through my research projects and this thesis. I would also like to thank my second supervisor Professor Timo Jääskeläinen and I wish to thank Metla for giving me an opportunity to finish my thesis.

I'd like to express my gratitude to my colleagues; Alexey Andriashing, Pauli Fält, Ville Heikkinen, Jouni Hiltunen, Tuija Jetsu, Oili Kohonen, Juha Lehtonen, Jarkko Mutanen, Joni Orava, and Paras Pant for creating a very good working ambiance. I'd like to give special respect to Jussi Kinnunen who shared the same working room with me for many years and helped me through many problematic issues. Also, I would like to thank Tapani Hirvonen for his supportive work and very nice working trips to Korkeakoski.

I am grateful to all my co-authors but, I'd like to especially thank authors Adam Herout, Jiří Havel, Radovan Jošth and Pavel Zemčík in Brno for very good and productive co-operation.

I'd like to thank my friends Aki Pulkkinen and Ville Pietikäinen for helping me during my university studies and I'd like to especially thank Aki for good comments and ideas for the thesis. Also I would like to thank my parents Reijo and Päivi for their support.

Finally, special thanks go to my wife Minna for her encouragement, support and love.

Joensuu March 15, 2012 *Jukka Antikainen*

LIST OF PUBLICATIONS

This thesis is based on the author's work in the field of spectral color research and the following selection of the author's publications:

P1 Jukka Antikainen, Markku Hauta-Kasari, Jussi Parkkinen and Timo Jääskeläinen, "Using two line scanning based spectral cameras simultaneously in one measurement process to create wider spectral area from the measured target", *In Proceedings of IEEE International Workshop on Imaging Systems and Techniques* (IST07), Krakow, Poland, May (2007).

P2 Jukka Antikainen, Jussi Kinnunen, Tapani Hirvonen and Markku Hauta-Kasari, "Heartwood Detection for Scotch Pine Using Fluorescence Image Analysis", accepted 23.1.2012 to *Holzforschung* (2012).

P3 Jukka Antikainen, Joni Orava, Mikael von und zu Fraunberg, Markku Hauta-Kasari and Juha E Jääskeläinen, "Spectral imaging of neurosurgical target tissues through operation microscope", *Optical review*, vol. 18, no. 6, pp. 458–461, (2011).

P4 Jukka Antikainen, Markku Hauta-Kasari, Timo Jääskeläinen and Jussi Parkkinen, "Fast Non-Iterative PCA computation for spectral image analysis using GPU", *In Proceedings of 5th European Conference on Colour in Graphics, Imaging, and Vision, IS&T* (CGIV10), Vol 5, pp. 554–559, Joensuu, Finland, June 2-3, (2010).

P5 Jukka Antikainen, Jiří Havel, Radovan Jošth, Adam Herout, Pavel Zemčík and Markku Hauta-Kasari, "Non-Negative Tensor Factorization Accelerated Using GPGPU", *IEEE Transactions on Parallel and Distributed Systems*, pp. 1135–1141, January 1, (2010).

These original publications have been included at the end of this thesis with the permission by their copyright holders.

SUMMARY OF PUBLICATIONS AND AUTHOR'S CONTRIBUTION

The publications selected in this dissertation are original research papers on spectral imaging and analysis.

Paper **P1** contains a spectral imaging method for measuring visible and near-infrared regions simultaneously. The developed method was used for determining moisture content from wood samples. The idea for the paper came from the author. All the measurement software, the measurements, as well as the data analysis were made by the author. The author was also responsible for writing the article, although co-authors gave comments for the paper.

Paper **P2** describes a novel method of heartwood detection for Scots Pine. The proposed heartwood detection is based on fluorescence imaging and various computational methods. Fluorescence imaging is based on bispectral measurements which are made by using a bispectrometer. The paper also proposes an online measuring prototype for determining the heartwood content in a real industrial environment. The idea for the paper came from the author and Jussi Kinnunen MSc. The author developed the prototype and all the necessary codes for measurements and data analysis. The author wrote 95% of the paper and Tapani Hirvonen MSc wrote 5%. All the co-authors gave comments for the paper.

Paper **P3** presents a compact spectral imaging system used to image neurological targets. The device is connected directly to a surgical microscope used during operations. The Principal Component Analysis (PCA) was tested for discriminating between neoplastic and healthy tissues. The idea for the paper was raised during discussions between the author and co-authors. The measuring system was developed by the author and Joni Orava PhD. The author did all the programming and experimental work for the measuring system and all the data analysis for the measurements. The author wrote 90% of the paper and the co-authors wrote the remaining 10%. All co-authors gave necessary comments for the paper.

Paper **P4** contains a GPU implementation of Principal Component Analysis. The paper proposes an implementation which can be used to speed-up the computational process of PCA. The computational efficiency of the implementation was tested with spectral images of different sizes. The idea for the paper was generated by the author. The author wrote all the codes and made all the experimental tests. The paper is fully written by the author. Co-authors gave comments for the paper.

Paper **P5** contains an implementation of Non-Negative Tensor Factorization (NTF) for spectral image processing by using Graphics Processing Units (GPUs). The paper proposes an implementation which provides remarkable speed up for the computation of NTF. This was tested with several spectral images of different sizes. The idea for the paper was generated by the author. Jiří Havel MSc did the programming work and the experimental testing. The author wrote 50% of the paper. The rest of the paper was written by co-authors, particularly by Dr. Adam Herout and Jiří Havel MSc. All co-authors gave comments for the paper.

LIST OF ABBREVIATIONS

PCA	Principal Component Analysis
NTF	Non-negative Tensor Factorization
RGB	Red, Green and Blue color system
CFA	Color filter array
GPU	Graphics Processing Unit
CPU	Central Processing Unit
ALU	Arithmetic Logic Unit
FWA	Fluorescent whitening agent
PGP	Prism-Grating-Prism element
LCTF	Liquid Crystal Tunable Filter
AOTF	Acousto-Optic Tunable Filter
CCD	Charge-coupled device
ICCD	Intensified CCD camera
EMCCD	Electron Multiplying CCD camera
ALA-5	5-aminolevunilic acid

Contents

1 Introduction

Color representation and formation are usually based on the red, green and blue (RGB) color component system [1]. RGB color representation is derived from the basics of the human visual system [2]. Every color which is produced on television, or digital cameras etc., are formed by mixing these three base colors. One problematic issue with the three color component system is *metamerism* [3].

With metamerism, two different colors may look the same under one illumination, but different under another. An example of metamerism comes from the textile industry: a customer wants to buy black trousers, which match a black jacket. In the shop, the color of the trousers may look to be the same as the jacket, but under outdoor illumination the color of the trousers may look dark blue and the jacket black. The three color component system is not accurate enough for detecting these differences under one light source. However, the problem of metamerism can be solved by using a spectral approach [3].

Spectral information holds the most accurate representation of color. The color of the target material can be described by a high number of color channels. For example, when the color of the target is measured from 380 to 780 nm using 5 nm steps, the color information is described by 81 different color components. This information can be used to simulate the color under different light sources. With the spectral approach, metameric pairs can be detected more easily than with the normal three color component system.

Color and its accurately defined spectral information is increasingly becoming an important factor in many industrial applications, such as; the mineral industry [4], paper industry [5], wood industry [6–8], food quality control [9–11], and many other important areas [12–15]. The usage of spectral color information is also growing in the field of medical applications. Spectral information is used for; cartilage analysis [16], retinal image analysis [17], tumor

demarcation [18–20], and other medical fields [21,22]. Spectral measurements also provide an efficient tool for old art conservation and other analysis tasks as well [23,24]. The words *multispectral* and *hyperspectral* are also sometimes used in the literature in place of the term *spectral*.

A spectral image differs from a normal RGB-image by each pixel in the image holding full spectral information instead of just the three basic colors. Because of the large number of different color channels, the size of one spectral image can increase to several gigabytes. Therefore, the analysis of spectral data can be difficult and time-consuming. Thus, this dissertation also introduces faster implementations of well-known computational techniques for high dimensional data. For some target uses, especially in industry, the image analysis should be fast, or even real-time.

There are three objectives to the thesis. The first objective is to review the benefits and drawbacks of different spectral imaging methods and systems and this review forms an important part of the thesis. The second objective is to develop new spectral measuring methods and systems for industrial targets. Two new measuring methods for the wood industry are proposed. The first method is related to the determination of the moisture content of the wood boards and the second is related to measurements of the heartwood of *Scots Pine* by using fluorescence imaging. The developed spectral imaging system is also presented for a medical application. The third objective is to generate a faster implementation of spectral image analysis algorithms that are in general use. Implementations of *Principal Component Analysis* (PCA) and *Non-negative Tensor Factorization* (NTF) are done using *Graphical Processing Units* (GPUs).

In this thesis, Chapter 2 brings out the research problems addressed in this thesis. Chapter 3 describes the basics of spectral color and fluorescence. In Chapter 4, the structure of the spectral image and associated common methods are reviewed. Chapter 5 introduces two generally used mathematical methods: PCA and NTF for spectral image analysis. Chapter 5 also describes fast implementations for the discussed mathematical methods. Chapter 6

describes and summarizes the main results and achievements of the published papers. Finally, Chapter 7 concludes the results of this thesis and discusses possible future research topics.

2 Research problems addressed in this thesis

The research problems related to spectral image acquisition and analysis in this thesis are as follows:

- Spectral cameras for wide spectral regions do not exist, because single sensor cameras for wide spectral ranges are not available. The requirement for simultaneous spectral image acquisition from visible and infrared regions came from the wood industry, in which the humidity of wood was the property of interest. The samples needing to be measured were frozen and, as the samples would melt between different camera measurements, simultaneous measurement was needed.

- As yet, an image acquisition system for measuring the heartwood content of wooden material from fresh and dried samples does not exist. The need for heartwood content measurement came from the wood industry, where the heartwood content needs to be measured as the production line is moving.

- One research problem arose in the medical field. As yet, spectral image databases from neurosurgical targets are not available. Only a small number of spectral images have been taken in [18, 19]. In this thesis we needed to design and implement a spectral imaging system for neurosurgical targets. The spectral information from healthy tissues and tumors was a region of interest to medical experts at the university hospital, especially the enhancement of the margin between healthy and neoplastic tissues.

- Spectral images contain huge amounts of data and efficient analysis requires fast computational methods, especially in

real world applications. To visualize spectral image data, different representations can be used. Especially in medical applications, the spectral image acquisition and analysis need to be carried out in near real-time. In this thesis, two well-known computational methods were selected in order to study their performance in near real-time. It is known that the NTF calculation is time consuming and seeing results in near real-time would provide new possible applications, for example, in neurosurgical applications where the surgeon must see the results during surgery in near real-time.

The research problems were addressed as follows:

- A spectral image acquisition system was realized using two spectral cameras simultaneously in the visual and infrared regions. The system was tested in a research project with hundreds of wooden boards. Because the humidity of an object can be seen from the infrared area, it is possible to use this system in moisture-content related studies.

- A new measuring system for heartwood detection based on fluorescence was designed and implemented in this thesis. This phenomenon was confirmed by an accurate bispectral measurement from which the optimal illumination and detection wavelengths were obtained. By this method, the heartwood content from both fresh and dried samples can be detected. The cooperative company has applied patents [25, 26] for the measuring system.

- A spectral imaging acquisition system was designed and connected to the neurosurgical microscope at Kuopio University Hospital. The proposed system is smaller than that in Ref. [19] and can be used during surgery without disturbing the surgeon. Spectral images were collected from ten different surgical procedures and a total of 38 spectral images were acquired. Preliminary analysis for tissue separation was carried out.

- Two fast implementations for spectral image analysis were realized. Both of the implementations were planned for the Graphical Processing Unit (GPU) and were realized using the C++ language. PCA implementation produced an increase in speed of about $7\times$ and NTF implementation an increase of $60 - 100\times$ when compared to CPU.

3 Spectral color

Digital color is normally defined in some *trichromatic color space* like RGB. Each color is formed by a combination of these three base colors. Electronic devices such as computer displays and digital cameras use the three color component system to produce colors. *Spectral color* is an extension to the normal trichromatic color system. In spectral color space each color is formed by using tens, or even hundreds of different color components.

3.1 ELECTROMAGNETIC SPECTRUM

The *color spectrum* is an electromagnetic wave that can be represented as a function of wavelength or frequency [27, 28] and the shape of this spectrum determines the color that is sensed. *Visible light* for the human eye is only a small fraction of the entire electromagnetic radiation spectrum. The electromagnetic spectrum is categorized into different wavelength regions as shown in Fig. 3.1.

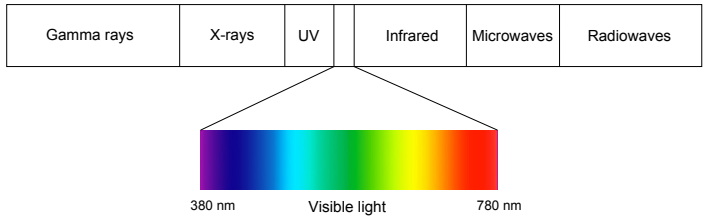

Figure 3.1: Electromagnetic spectrum.

The *human visual system* is very limited and it can only detect a small region of the electromagnetic spectrum from 380 to 780 nm. Therefore, the human visual system cannot detect other wavelength regions such as *ultraviolet* (UV) or *infrared* (IR). The spectral approach makes it possible to use ultraviolet and infrared regions as well. These unseen regions provide very important features of the

target material. Figure 3.2 shows example measurements when the infrared region could provide important information about an object such as moisture content. In the infrared region, water absorption peaks at 970 nm, 1190 nm and 1450 nm and can be recognized and used for moisture determination [29]. The visible region of the color spectrum cannot be used to determine the moisture content, whilst the infrared region provides good contrast between dry and moist wood.

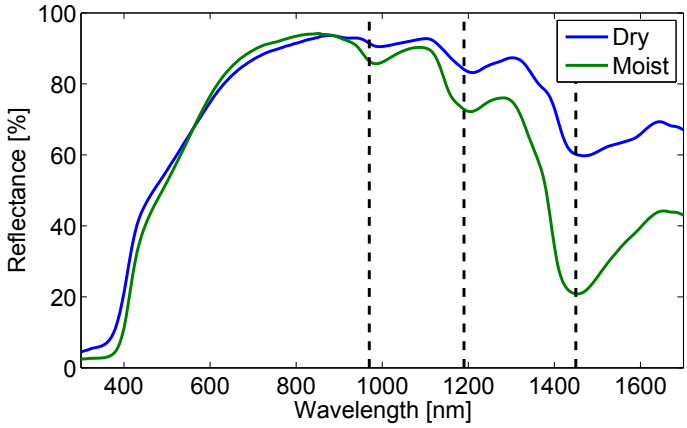

Figure 3.2: Reflectance spectra of dry and moist Scots Pine sample. Black dashed lines are the water absorption peaks.

Resolution of the measured spectra is usually between 1 to 20 nm depending of the measuring device and the usage of the information. A single color spectrum $\mathbf{s}$ can be defined as a vector:

$$\mathbf{s}(\lambda) = [s(\lambda_1), s(\lambda_2), \ldots, s(\lambda_n)]^T, \tag{3.1}$$

where λ is the wavelength and n is the number of wavelength channels in the spectrum. The optimal resolution and the sampling interval for color spectra has been studied by Juha Lehtonen [30].

3.2 FLUORESCENCE

Fluorescence is a phenomenon where a material re-emits the absorbed light at a longer wavelength and with a lower energy level. Usually, fluorescence occurs when the target is exposed to *ultraviolet radiation*. Ultraviolet radiation can be divided into three main categories; UV–C (100–280 nm), UV–B (280–315 nm), and UV–A (315–400 nm) [31]. Fluorescent colors are widely used in various areas such as security markings, the paper industry, and textile industry. For example, *fluorescent whitening agents* (FWA) are used in the paper industry to produce white paper [5, 32]. The whitening agent absorbs the ultraviolet light, and re-emits it in the blue region of the spectrum. Without the whitening agent, the raw paper would look brownish.

Fluorescence can be measured by using a *bispectrometer* device [33] where the material is illuminated by a narrow band of monochromatic light and the *emission* wavelength is measured with a spectrometer. The *excitation* wavelength region is scanned through the whole inspected area. This method is called a *double monochromator method* [34].

From bispectral measurements, a *Donaldson matrix* [34] can be formed. The Donaldson matrix describes the relationship between the excitation and emission wavelengths of the fluorescence (Fig. 3.3).

Fluorescent colors are a very good example of why the selection of illumination is critical in color perception and for the color measurements. Figure 3.4a shows an example where a set of fluorescence standards are illuminated with a visible light and with a UV-light source 3.4b. Figure 3.5 shows the Donaldson matrix from the blue green fluorescent standard (upper center), which is measured with the bispectrometer device. These fluorescent standards are used for measuring device calibration and for the development of optically brightened materials.

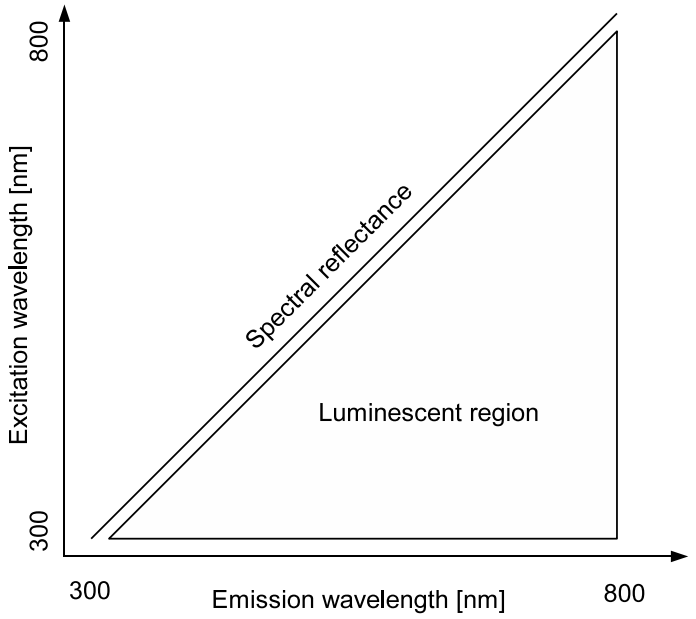

Figure 3.3: Donaldson matrix.

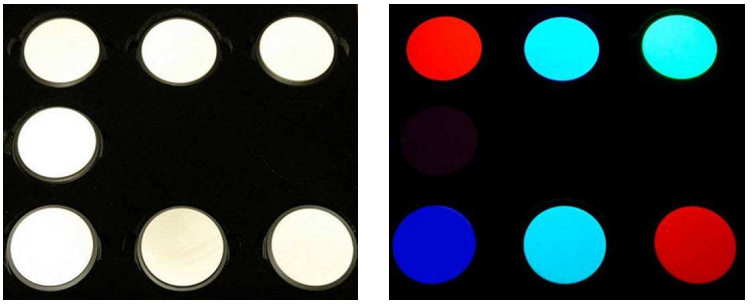

Figure 3.4: (a) Fluorescent color standards under the daylight (D65) illumination. (b) Fluorescent color standards under UV–illumination. (Photographs by Jussi Kinnunen)

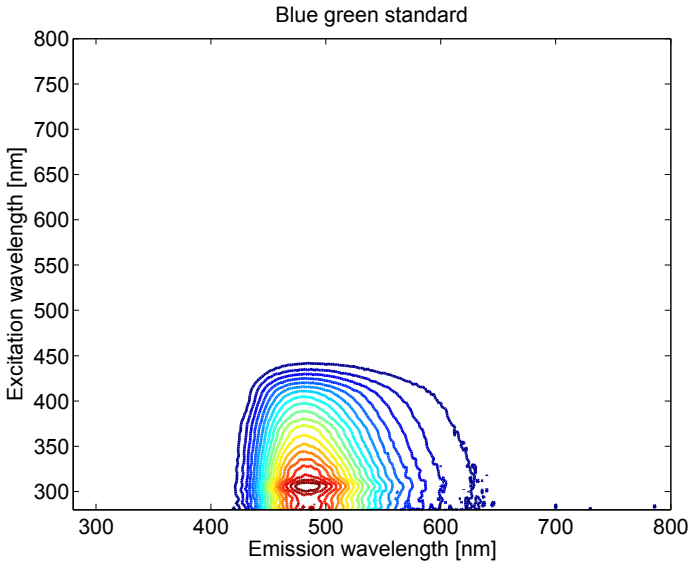

Figure 3.5: Donaldson matrix from blue green fluorescent standard (upper center).

4 Spectral imaging

In normal color imaging each color is captured by using three primary colors. Colors in a normal digital *charge-coupled device* (CCD) -cell are captured through a *color filter array* (CFA). The most common CFA is a three color Bayer filter (Fig. 4.1a) where each color is formed through red, green and blue filters [35]. Sony has also introduced a CCD-cell where one of the green filters is replaced with an emerald filter (Fig. 4.1b) to achieve four-primary cameras [36]. Researchers have also introduced a six-primary HDTV-video camera by combining two CCD-cells in one imaging process [37]. In addition, there are commercial devices incorporating 3 CCD sensors [38].

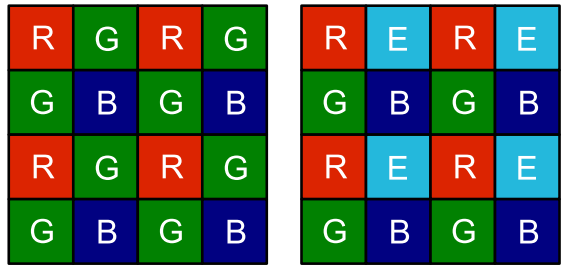

Figure 4.1: (a) 3-color filter. (b) 4-color filter.

In the case of spectral imaging, each pixel contains a color spectrum with tens, or hundreds of color channels. As with normal digital images, the spectral image can contain information from the visible part of the spectrum, but also it can be extended to unseen wavelength regions such as ultraviolet and infrared.

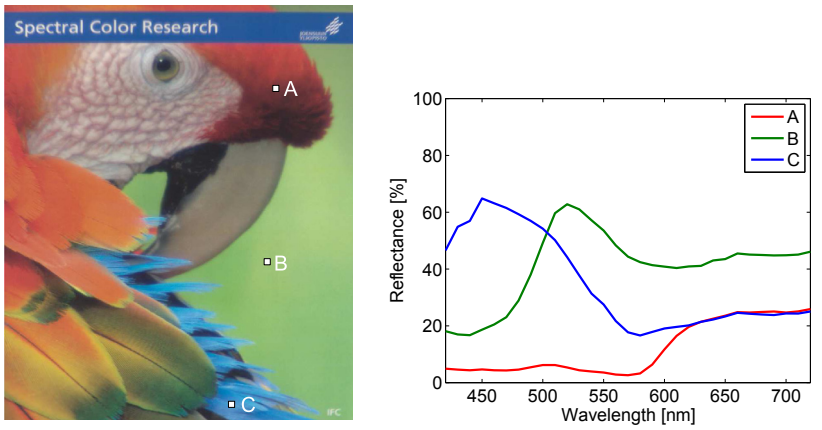

(a) (b)

Figure 4.2: (a) Spectral image converted to RGB space and three selected points. (b) Reflectance spectra of the selected points.

4.1 STRUCTURE OF SPECTRAL IMAGE

The RGB image contains three gray scale channel images (Fig. 4.3(a)) which are acquired through 3 filters, as illustrated in Figure 4.3(b). The spectral image can contain multiple gray scale channel images (Fig. 4.4(a)), which can be acquired through narrow band filters shown in Figure 4.4b). When the spectral image is captured by using the 400 to 700 nm region by 10 nm steps, the image consists of 31 different gray scale channel images. Each channel image contains information about one narrow spectral channel band. The spectral image can be converted to other color spaces such as RGB using common conversion algorithms [1,27].

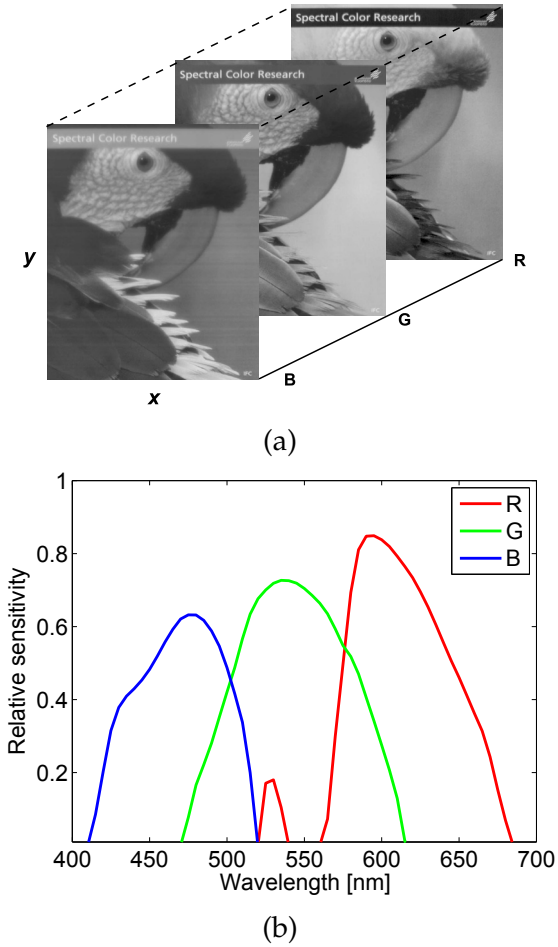

Figure 4.3: (a) Structure of RGB image. (b) Spectral sensitivities of one RGB camera.

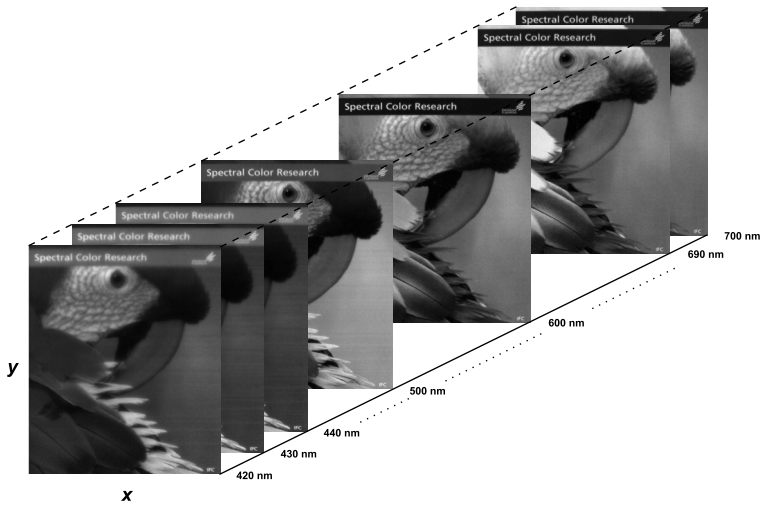

(a)

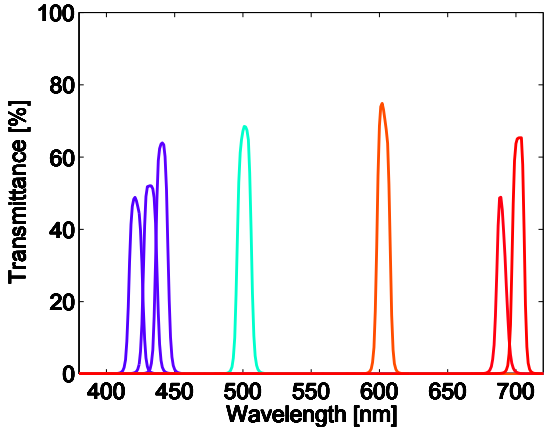

(b)

Figure 4.4: (a) Structure of spectral image. (b) The spectral transmittances of filters corresponding the wavelengths in a).

Because of the large amount of color information, the storage size of a spectral image can rise to hundreds of megabytes, or even to gigabytes. Usually, these images are saved to user specific binary formats [39]. In some case, compression methods like PCA are used to reduce data dimensionality [40]. However, currently there is no standard file format available for saving spectral images.

4.2 IMAGING TECHNIQUES

Spectral image acquisition can be done using three different approaches. In the first approach, the spectral image is captured line by line [12]. Each pixel on each single line contains the full spectral information of the target. The spatial domain can be captured by moving the target or the camera. In the second method, the spectral image is captured by using a filter, for example, a Liquid Crystal Tunable Filter (LCTF) [41]. Each channel image is captured with a different filter transmittance. This approach captures x and y spatial domains at once for each wavelength channel. In the third approach, the spectral image is formed by capturing the spectral and spatial domains at the same time [42]. The measured image is divided into multiple sub images by using optical elements. A different wavelength region with full spatial information goes to different places on the CCD-cell. The spectral image can be reconstructed from the divided sub images.

Each method has its own benefits. The first approach is much better for industrial line applications where targets cannot be stopped and where the imaging has to be done in real time, as in a conveyor belt production. The second approach provides quite fast image capture, but the spectral resolution is not as good as in the first approach and it is not so convenient for moving targets. However, the scanning of the camera or the object is not needed. The third approach is the fastest, but usually the spatial or the spectral resolution is poor.

4.2.1 Line scanning

Line scanning based spectral cameras mainly consist of *ImSpector direct sight spectrographs* [12, 43]. The structure of the spectral camera is described in Figure 4.5. The main technique of the direct sight spectrograph is based on a single *prism-grating-prism* (PGP) element. The incident light is controlled through a narrow slit to the PGP element. The PGP element disperses the light to a matrix detector like a CCD–cell. The spatial information from the measured line is drawn to the x-axis and spectral information to the y-axis on the detector. To capture the full spatial information of the target, the position of the line must be changed either by moving the camera or the target. Scanning can be also done by using a rotation mirror.

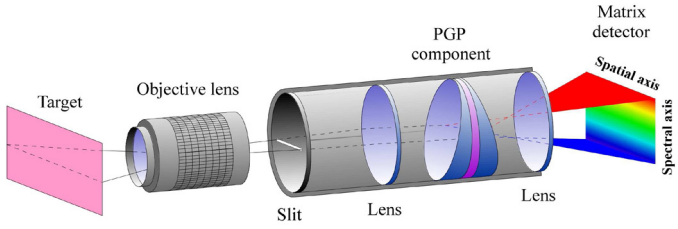

Figure 4.5: Structure of direct sight spectrograph (drawn by Jouni Hiltunen).

Line scanning based on a direct sight spectrograph provides high spectral resolution and it can be also used for capturing high quality spatial information. One drawback of the imaging system for laboratory use is the measuring speed. Moving the target or the camera can take some time and if high spatial resolution is needed, the measuring time can increase to several tens of minutes. However, the imaging system is very applicable to industrial lines where measured targets are constantly moving and the level of illumination can be high. The exposure time is directly proportional to the level of light. If a smaller exposure times can be used, the total imaging time will be greatly decreased. Figure 4.6 shows a spectral

imaging system [44], which has been developed and used at the University of Eastern Finland for scientific purposes.

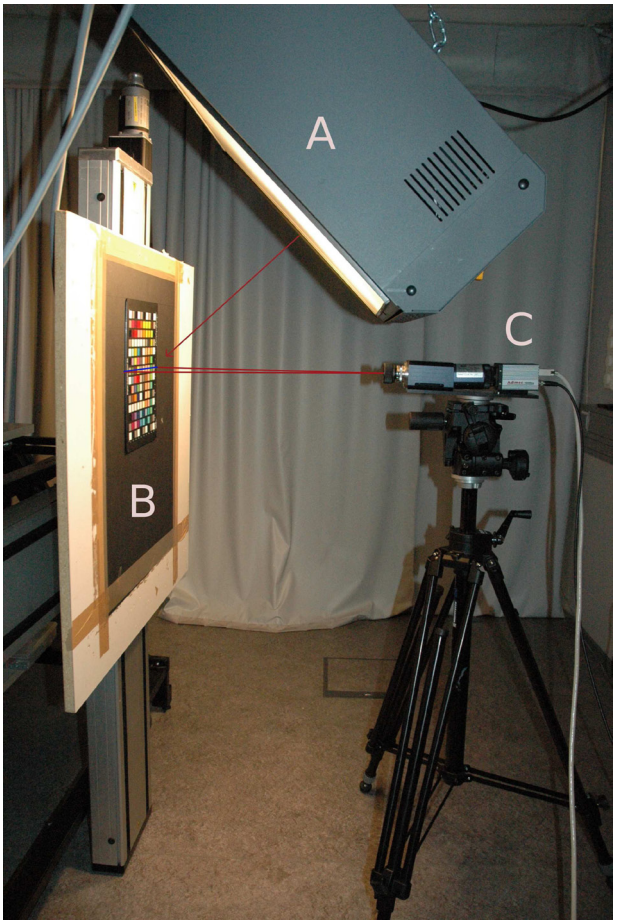

*Figure 4.6: Line scanning based spectral imaging system. **A** is the light source, **B** is the sample table and **C** is the camera.*

4.2.2 Spectral channel based

The spectral image can be captured in the spectral domain by using various filters and optical systems, such as; a *Liquid Crystal Tunable Filter* (LCTF) [41], an *Acousto-Optic Tunable Filter* (AOTF) [45], an *interference filter* [1], and an *interferometric* spectral imaging system [42,46].

In the Lyot type of LCTF, the spectral band selection is done by tuning the liquid crystals in the filter with an electric field. The Lyot filter is a pack of liquid crystal plates and linear polarizers. Different wavelength transmittances of the filter are achieved by tuning the position and the angle of the liquid crystals and polarizers [47].

The AOTF is controlled by the acoustic waves of radio frequencies. The AOTF is built from a crystal element, which is vibrated with different sonication frequencies. Varying the sonication frequency gives control of the desired wavelength of transmittance of the crystal [45,48].

In an interference filter based imaging system, a mechanical filter wheel with several separate filters is rotated in front of the CCD camera. Each filter has a different wavelength transmittance and the spectral information is obtained sequentially by capturing images through the different filters [1].

The interferometric spectral imaging system can obtain multiple spectral images at the same time. Wavelength information with spatial information of the whole area is divided into the matrix detector by using various optical components [42,46,49,50]. Spectral resolution of the interferometric imaging system is a trade-off of the spatial resolution. If the spectral resolution increases, the spatial resolution decreases, and vice versa. Examples of the technical details for the typical spectral imaging techniques are presented in Table 4.1.

Table 4.1: Characteristics for typical spectral imaging techniques.

	PGP	**LCTF**	**AOTF**	**Interference**	**Interferometric**
Scanning direction	Spatial	Spectral	Spectral	Spectral	Spectral/Spatial
Scanning type	Mechanical	Electrical	Electrical	Mechanical/filter wheel	Electrical
Spectral resolution	1 - 20 nm	7 - 20 nm	2 - 20 nm	10 - 80 nm	5 - 30 nm
Spatial resolution	Scanning dep.	Sensor dep.	Sensor dep.	Sensor dep.	Sensor/grating dep.
Channels	11 - 121	6 - 51	6 - 91	4 - 24	32 - 128
Available area	200 nm - 12 μm	400 - 2450 nm	250 - 1700 nm	193 - 1650 nm	300 - 1120 nm
Acquisition speed	Good	Slow	Fast	Slow	Really fast
Light sensitivity	Good	Low	High	Good	Good
Price	Expensive	Expensive	Very expensive	Cheap	Expensive

See refs. [42, 43, 46, 50–53]

4.2.3 Properties of the imaging system

An industrial environment has specific requirements of a spectral imaging system. The environment might be dusty, or the system might be affected by heavy vibration. In some cases, the level of light might be the problem. A total response of the imaging system is formed from the different factors and these need to be considered individually for each application. These factors are; the sensor sensitivity, the light source, possible filters, and optics, etc. The total response $S(\lambda)$ for the imaging system can be formulated as follows:

$$S(\lambda) = \int_{\lambda_{min}}^{\lambda_{max}} L(\lambda)R(\lambda)F(\lambda)s'(\lambda)o(\lambda) + n, \tag{4.1}$$

Above $L(\lambda)$ is the light source, $R(\lambda)$ is the reflectance $r(\lambda)$ or the transmittance $t(\lambda)$ of the target, $F(\lambda)$ is the transmittance of the filter, $s'(\lambda)$ is sensitivity of the detector, $o(\lambda)$ is the transmittance of the optics and n is an additional noise of the system. Table 4.2 shows advantages and disadvantages of common PGP and LCTF imaging systems.

Table 4.2: Advantages and disadvantages for PGP and LCTF imaging systems.

	PGP	**LCTF**
$L(\lambda)$	Line illumination can be used	Homogeneous light preferred to whole area
$t(\lambda)$	Very good	Poor/Acceptable
$r(\lambda)$	Surface curvature causes problems	Good for non-flat objects
$s'(\lambda)$	Good	Poor
$o(\lambda)$	Good	Good
n	Not a problem	Poor filter transmittance on blue region cause noise

There is no use for a UV sensitive sensor if the optics or the filters do not transmit UV-radiation, and vice versa. The amount of UV-radiation might be a problem in fluorescence imaging applications. If the light source used does not produce enough UV-radiation, then the intensity level of the fluorescence may be too low to be detected. In low level light applications, Intensified CCD (ICCD) cameras, or Electron Multiplying CCD (EMCCD) cameras [54] can

be used. Similar problems can also be detected in the case of infrared imaging.

Different filters and sensors have their own spectral responses at specific wavelength regions. For example, the visible area LCTF component has very poor transmittance levels in the purple and blue region ($400 < \lambda < 470nm$) of the spectrum (Fig. 4.7).

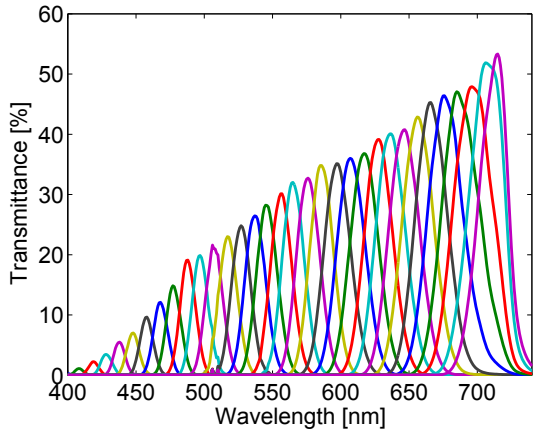

Figure 4.7: Measured spectral transmittances of VariSpecVis LCTF component.

Different light sources produce different spectral power distributions (Fig. 4.8). If an LCTF component is used with a *tungsten light source* (A), the blue region of the spectrum cannot be efficiently detected. The combination of the filter and the tungsten light source works better in the red region of the spectrum. The *daylight source* (D65) provides a daylight illumination and this is more useful in the blue region than the tungsten light source. The *fluorescent light source* (F11) is very peaky and it is not commonly used for reflectance measurements.

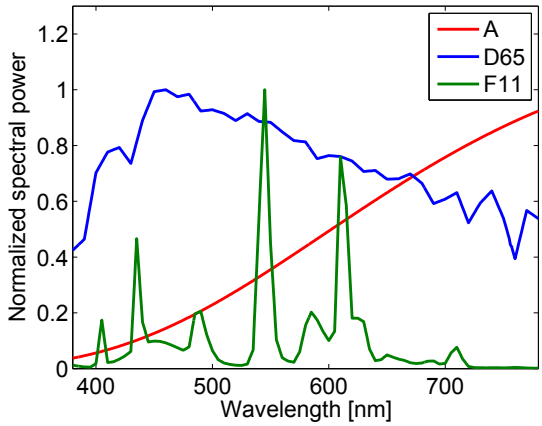

Figure 4.8: Normalized spectral power distributions for A, D65 and F11 light sources.

5 Spectral image analysis

A spectral image can contain large amounts of information and therefore spectral image analysis is usually very time-consuming. Some of the potential industrial applications related to spectral imaging cannot practically be done because of the slow processing times. Therefore, it is necessary to speed up the commonly used analysis algorithms. Because of the slow processing times of a general Central Processing Unit (CPU), the implementation of a Graphical Processing Unit (GPU) for the algorithms has been studied. This chapter describes two well-known spectral image analysis algorithms and how they can be implemented with a GPU.

5.1 PRINCIPAL COMPONENT ANALYSIS

Principal Component Analysis (PCA) is a widely used statistical method used to reduce the dimensionality of a dataset [55]. For spectral image analysis, PCA can be used for compression by reducing the dimensionality of the wavelength channels of the image and it can also be used for extracting interesting features from the images. Use of PCA for spectral image analysis has been studied in various papers [23, 40, 56–60]. The PCA computation can be undertaken using covariance or correlation matrices [61]. In the sense of spectral image analysis, centering the data is not commonly used. The formation of the PCA for spectral image analysis is as follows: the spectral image is converted to a two-dimensional matrix **S** where each column contains the spectrum of a single pixel of the spectral image

$$\mathbf{S} = \begin{pmatrix} s_1(\lambda_1) & \dots & s_m(\lambda_1) \\ \vdots & \ddots & \vdots \\ s_1(\lambda_n) & \dots & s_m(\lambda_n) \end{pmatrix}. \tag{5.1}$$

Here, m is the number of pixels in the spectral image and n is num-

ber of wavelength channels. A correlation matrix **R** can be computed by using equation

$$\mathbf{R} = \frac{1}{m}\mathbf{S}\mathbf{S}^T. \tag{5.2}$$

The eigenvectors Φ_i and eigenvalues σ_i for matrix **R** are from equation

$$\mathbf{R}\Phi_i = \sigma_i\Phi_i \tag{5.3}$$

Eigenvalues σ_i and eigenvectors Φ_i are ordered such that the eigenvalues are in descending order. A new matrix **B** is defined by taking the k first eigenvectors as

$$\mathbf{B} = (\Phi_1, ..., \Phi_k) \tag{5.4}$$

Inner product images **P** are calculated by using the selected base vectors **B** and the previously defined 2D matrix **S** by

$$\mathbf{P} = \mathbf{B}^T\mathbf{S}. \tag{5.5}$$

Now the spectral image can be reconstructed using the inner product images and the corresponding eigenvectors. Reconstruction of the spectral image is calculated with an equation

$$\tilde{\mathbf{S}} = \mathbf{B}\mathbf{P}, \tag{5.6}$$

where $\tilde{\mathbf{S}}$ is a reconstructed spectral image of the same size as S, but it is represented by using a fewer number of principal components. Many algorithms can be formulated to operate on the **B** and **P** matrices, which are smaller than the original image **S**. This can result in a speed-up of the image processing time.

5.2 NON–NEGATIVE TENSOR FACTORIZATION

Non-Negative Tensor Factorization (NTF) is another commonly used spectral image analysis method. It has been used in many different areas such as; global climate analysis, neuroscience, and image

processing [62–66]. For spectral image analysis, NTF is used for compression [58], optimal filter selection [13,67] and feature extraction [68]. The NTF produces positive base vectors which can be used as filters. These filters can be manufactured and used in real optical systems [13].

Let $\mathbf{G}$ be a size of $x \times y \times z$ nonnegative third order tensor. The non-negative tensor factorization of $\mathbf{G}$ can be solved by using non-linear minimization problem

$$\min_{\hat{\mathbf{G}} \geq 0} \|\mathbf{G} - \hat{\mathbf{G}}\|_F^2 \tag{5.7}$$

where $\hat{\mathbf{G}}$ is a reconstructed data and $\|A\|_F^2$ is the square Frobenius norm. The rank-K reconstruction is defined as a sum of tensor products

$$\hat{\mathbf{G}} = \sum_{k=1}^{K} \mathbf{u}^k \otimes \mathbf{v}^k \otimes \mathbf{w}^k, \tag{5.8}$$

where $\mathbf{u}^k$, $\mathbf{v}^k$ and $\mathbf{w}^k$ are basis vectors of non-negative values. This reconstruction process for third order tensor factorization is illustrated in Figure 5.1.

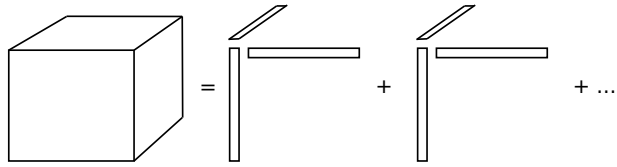

Figure 5.1: Illustration of third order tensor factorization by using sums of rank-1 tensors.

The main approach to non-negative tensor factorization is based on the Block Gauss-Seidel (BGS) method [69]. Hazan *et al.* [67] derived a gradient descent method by combining Gauss-Seidel and Jacobi iterative update schemes where: u^k, v^k, and w^k are calculated using iterative steps (5.9)–(5.11)

$$u_i^k \leftarrow \frac{u_i^k \sum_{y,z} \mathbf{G}_{i,y,z} v_y^k w_z^k}{\sum_{m=1}^{K} u_i^m \langle v^m, v^k \rangle \langle w^m, w^k \rangle}, \tag{5.9}$$

$$v_i^k \leftarrow \frac{v_i^k \sum_{x,z} \mathbf{G}_{x,i,z} u_x^k w_z^k}{\sum_{m=1}^{K} v_i^m \langle u^m, u^k \rangle \langle w^m, w^k \rangle}, \tag{5.10}$$

$$w_i^k \leftarrow \frac{w_i^k \sum_{x,y} \mathbf{G}_{x,y,i} u_x^k v_y^k}{\sum_{m=1}^{K} w_i^m \langle u^m, u^k \rangle \langle v^m, v^k \rangle}, \tag{5.11}$$

where $\mathbf{G}$ is the dataset and $\langle , \rangle$ denotes the inner product. Iteration steps are repeated hundreds, or even hundreds of thousands times for convergence to the correct solution depending on the complexity of the dataset. Therefore, the iterative NTF computation is quite time-consuming and a method by which to speed it up would be useful.

5.3 FAST IMPLEMENTATIONS

GPUs offer a fast parallel computation platform. At first the GPU was developed for gaming purposes, but nowadays the efficiency of the GPU is used for scientific purposes as well. GPU architecture offers a highly parallel and multithreaded platform with high memory bandwidth [70]. The GPU is well suited for tasks where the same code can be executed simultaneously for multiple parts of the dataset such as image processing tasks.

Figure 5.2: Structures of the CPU and GPU architectures. [70]

The differences between CPU and GPU architectures are shown in the Figure 5.2. A normal CPU contains only four to eight *arithmetic logic units* (ALU) whereas the GPU can contain hundreds or even thousands. This is one of the reasons why the computational efficiency of the GPU is higher than CPU.

Each GPU contains multiple processors and each of those has their own individual registry and cache. Because of the different architecture, the GPU uses a different programming model than a normal CPU. The data is divided into a grid of blocks and each block contains up to 256 multiple threads (Fig. 5.3). Each thread executes the same code with different indexes. Each thread has its own private memory and each block has a memory which every thread can access. All the threads in a block can access the global memory of the GPU device. [70]

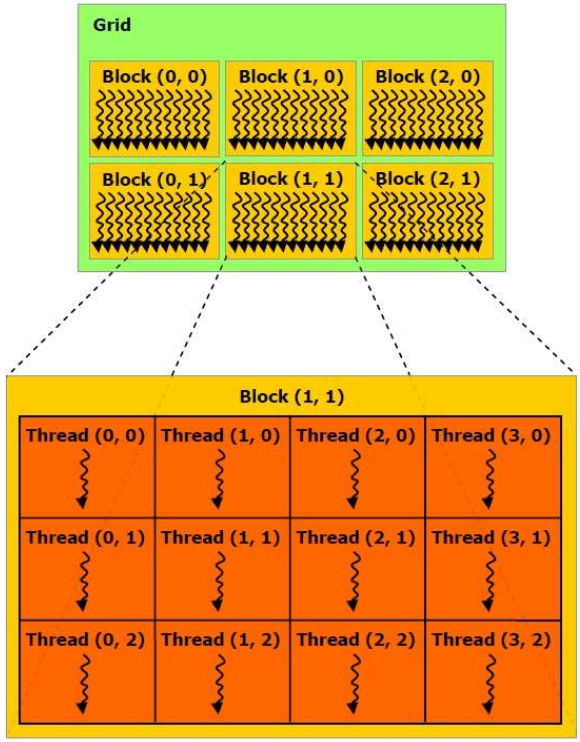

Figure 5.3: Principle of the programming architecture. [70]

Some parts of the PCA and NTF algorithms can be implemented very efficiently on a GPU. An algorithm and the time complexity of the PCA computation is described in Algorithm 1.

For the PCA computation, the most time-consuming parts are

Algorithm 1 An algorithm and the time complexity for the PCA.

Require: the input spectral image $\mathbf{S}$, wavelength count n, pixel count m, component count k

1: $\mathbf{S} \leftarrow \text{ConvertTo2D}(\mathbf{S})$ $O(nm)$
2: $\mathbf{R} \leftarrow (1/m)\mathbf{S}\mathbf{S}^T$ $O(n^2m)$
3: $[\Phi_i, \sigma_i] \leftarrow \text{SolveEig}(\mathbf{R})$ $O(n^3)$
4: $\mathbf{B} \leftarrow \mathbf{\Phi}(1:k)$ $O(kn)$
5: $\mathbf{P} \leftarrow \mathbf{B}^T\mathbf{S}$ $O(knm)$

the computation of the correlation matrix $\mathbf{R}$ and the inner product images $\mathbf{P}$. Time complexity for the matrix multiplication of two $n \times m$ matrices is $O(n^2m)$. The pixel count m determines the column count in matrix $\mathbf{S}$ and therefore the matrix column count might rise to hundreds of thousands and it is the main factor of the total computation speed. Time complexity for solving the eigenvalues and eigenvectors is $O(n^3)$ for most of the algorithms [71]. Computation time for solving the eigenvalues and eigenvectors is dependent on the count of spectral channels which is usually between 31 and 121. Therefore, this does not play such a big role in the total computation time. The GPU implementation is described with more details in the Paper **IV**.

Time complexity for a single NTF updating step can be derived from the iterative process. Let us consider equation 5.9, where the denominator is defined as $\sum_{m=1}^{K} \mathbf{u}_i^m \langle \mathbf{v}^m, \mathbf{v}^k \rangle \langle \mathbf{w}^m, \mathbf{w}^k \rangle$. Time complexity for the inner product of v is $O(y)$ and respectively for w the time complexity is $O(z)$. The scalar product and the summation are done K times, and therefore the time complexity for the computation of the denominator is $O(yK + zK)$. In the numerator part $\mathbf{u}_i^k \sum_{y,t} \mathbf{G}_{i,y,z} \mathbf{v}_s^k \mathbf{w}_t^k$, each value in the matrix layer G_i is multiplied with a scalar value, therefore the time complexity is $O(yz)$. The total time complexity for update step is then $O(yK + zK + yz)$. Time complexities for v and w are analogous to the complexity of u. For low rank-K tensors, it can be seen that the computation of the nominator is the most time-consuming part in the single update

step. The update step mainly consists of the repeated summations of large arrays, so basically it requires more memory bandwidth than computational efficiency.

Algorithm 2 An algorithm and the time complexity for the NTF.

Require: the input $\mathbf{G}$ (size $x \times y \times z$), the method rank K, and the iteration count I

Ensure: the output vectors u, v and w

1: Init u, v and w
2: **for** $i \in \{0, \ldots, I-1\}$ **do**
3: $\quad u \leftarrow \text{Update}_\text{u}(\mathbf{G}, u, v, w)$ $\quad O(yK + zK + yz)$
4: $\quad v \leftarrow \text{Update}_\text{v}(\mathbf{G}, u, v, w)$ $\quad O(xK + zK + xz)$
5: $\quad w \leftarrow \text{Update}_\text{w}(\mathbf{G}, u, v, w)$ $\quad O(xK + yK + xy)$
6: **end for**
7: **return** u, v and w

Algorithm 2 shows the structure of the iterative NTF computation. At first, the tensors u, v and w are initialized with random numbers between 0 and 1. Function $Update_j$ corresponds the update steps 5.9 - 5.11. The described algorithm does not ensure the convergence of the problem. The GPU implementation of the algorithm is described with more details in the Paper **V**.

6 Experimental cases

This chapter examines the experimental cases that were studied in this thesis. The first three sections describe three different measurement setups that were used in papers **P1 – P3** and the fourth section shows the results of the GPU implementations that were studied in papers **P4 – P5**.

6.1 WIDE SPECTRAL RANGE IMAGING

Sometimes, spectral information is needed from a wider wavelength region than one sensor or the optical system can provide. The measurements could be repeated with two different spectral cameras, or two spectral cameras could be combined in one measurement process. This way the measuring time will decrease and the measurement accuracy will be higher. The dual spectral camera measuring system is shown in Figure 6.1.

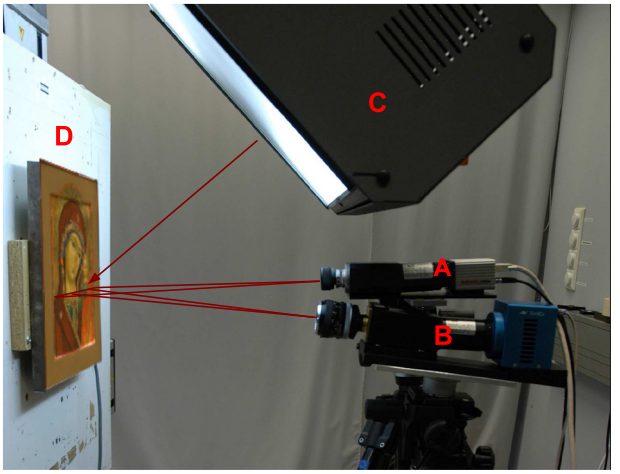

*Figure 6.1: Measuring setup for two camera system. Spectral camera (V10E) **A** measures on 400–1000 nm region. Spectral camera (N17E) **B** measures on 950–1700 nm region. **C** is a daylight simulator. **D** is a xy-sample table.*

The spectral cameras are placed vertically so that the camera for the visible range is attached on top of the infrared camera. Both spectral cameras are focused onto the same line on the surface of the target. The line is measured sequentially by both cameras. The difference between the measurements is only a couple of milliseconds. After the measurements, the sample is moved slightly to the next measuring position and the measurements are repeated until the whole spatial region is covered.

Spectral information has been used for moisture detection in wood. Most of the studies use reflectance spectroscopy measurements for determining the moisture content of the target. In the case of reflectance measurements, the moisture content of the wood sample can be detected only from the surface of the target. Paper **P1** proposed a dual spectral camera system for wood transmittance measurements in a laboratory environment (Fig. 6.2), which could be used for moisture detection.

The target application for the measuring system was a saw line. The main idea was to develop a system for spectral transmittance measurements for wooden boards. Initially the Scots Pine boards were frozen to simulate real winter circumstances on the saw line production. After the measurements were done for the frozen samples the measurements were repeated on thawed samples. In this way, the effect of the ice can be measured and quantified.

One problematic issue for the measurement process was heat. The hot light source started to thaw the samples almost immediately after the sample was placed in the sample holder. This problem was solved by performing the transmittance measurements simultaneously with both spectral cameras. If the measurements were done sequentially, the intensity level and the shape of the spectrum might have changed between the measurements, which would produce incorrect results.

The spectral imaging system reported in Paper **P1** has been used in many research projects. One of those projects studied the spectral analysis of old icons [23]. Spectral images were used to detect defects and hidden features of the icons. Because of the large size

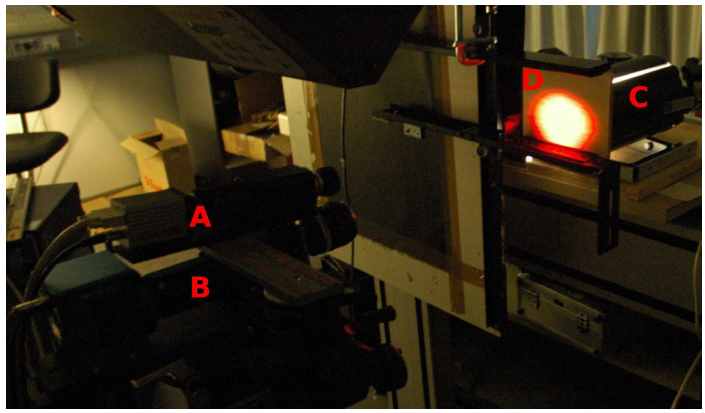

*Figure 6.2: Setup for wood transmittance measurements where **A** is V10E spectral camera, **B** is N17E spectral camera, **C** is Acclaim halogen lamp and **D** is a wooden board sample.*

of the icons, the acquisition time for a high resolution spectral image was long. The dual spectral camera system was used to speed up the measuring process. Spectral information for the icons was captured from 400 to 1700 nm by using both spectral cameras at the same time. For large icons, spectral measurements were done with multiple column images to achieve a good spatial resolution (Fig. 6.3).

Figure 6.3: Converted RGB slice images from large icon.

6.2 HEARTWOOD DETECTION FOR SCOTS PINE

Machine vision systems have an enormous role in the wood industry and they have been studied and used for detecting defects such as; knots, decay, blue stain etc., as well as log, sawn timber, and veneer sawing quality control [8, 72–77]. The heartwood detection of Scots Pine (*Pinus sylvestris*) has been studied with various methods like X-ray imaging [78] and thermal imaging [79, 80]. In addition, statistical approaches have been studied for estimating the heartwood content of the logs [81]. X-ray imaging offers accurate results for heartwood content, but usually the price for the system is high. X-ray scanning is mainly used for logs, but not for the final sawn products like boards.

Researchers have studied thermal imaging for heartwood detection [79, 80]. The idea of heartwood detection with a thermal camera is to compare temperature differences between the heartwood and the sapwood. Sapwood contains more water than heartwood and therefore the detection of the heartwood can be done. Consequently, the thermal imaging method cannot be used for dried samples [80].

Paper **P2** proposed a measuring method and system which can be used for fresh and dried samples. The measuring system is also low cost compared with an X-ray system. The proposed system is viable with logs and final sawn products. The main idea of the method is based on the fluorescence of stilbenes pinosylvin and its monomethyl ether [82]. These compounds are formed in the transformation of sapwood to heartwood [83] and they exist mainly in the heartwood with only very small quantities in the sapwood [84]. Therefore, the difference between the heartwood and sapwood can be detected by using the information given by the fluorescence. The amount of pinosylvin and its monomethyl ether correlates highly with decay resistance [82, 83, 85–89]. Therefore, the method could also be used for estimating the decay resistance of the final sawn products.

The accurate fluorescence measurements are described in the

Paper **P2**. It was seen that the heartwood (Fig. 6.4a) produced a fluorescence emission between 370 to 500 nm when 250 to 350 nm excitation wavelengths were used. The measurements show that the sapwood (Fig. 6.4b) does not produce such fluorescence in the same wavelength region.

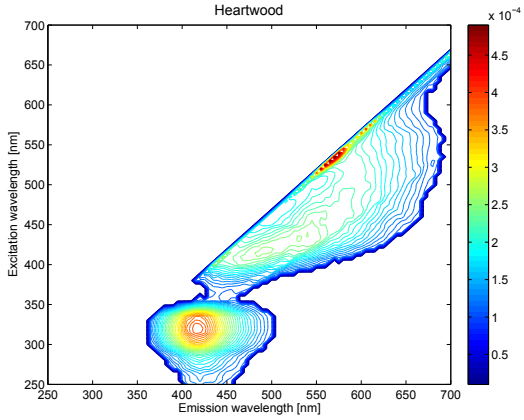

(a)

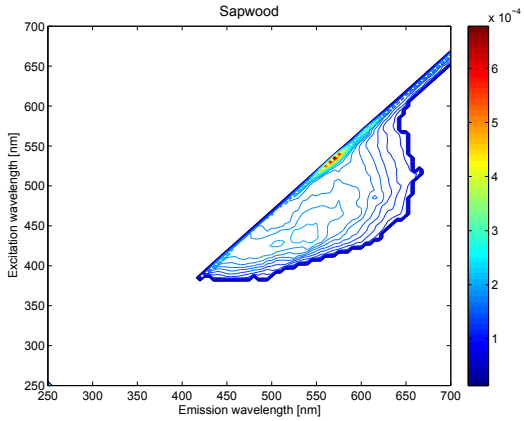

(b)

Figure 6.4: (a) Donaldson matrix from the heartwood fluorescence. (b) Donaldson matrix from the sapwood fluorescence.

From the fluorescence measurements, one narrow band interference filter (center WL = 420 nm, FWHM = 10 nm) was selected to enhance the differences between the heartwood and the sapwood.

Figure 6.5 shows the difference between the RGB image and the filtered fluorescent image.

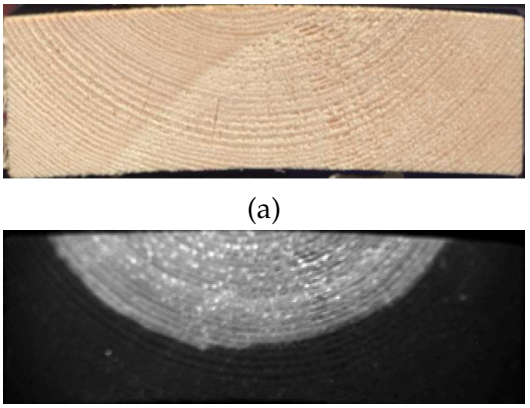

(a)

(b)

Figure 6.5: (a) RGB image of a sample. (b) Filtered fluorescence image of the sample (heartwood is shown as bright region).

The filtered fluorescence image can be used for determining the heartwood content of the sample. The actual image analysis is done using binary images. The original gray scale image is binarized by using two different threshold values. The first value is used for separating the board from the background and the second is used to separate the heartwood from the board. The relative amount of the heartwood can be calculated by comparing the areas of these binary images. A more detailed description of the algorithm is presented in Paper **P2**.

The Paper **P2** describes an online measuring system that is used in a manufacturing line. The measuring system is built in a Rittal rack. The system consists of a Retiga 4000DC monochrome camera (QImaging) with Nikkor lens (50mm, f=1.4). Fluorescence is excited by ten 11W UV-B light tubes. Reflected and emitted light is filtered with a narrow band interference filter (Oriel) to enhance the difference between the heartwood and the sapwood. The measuring point for each board is determined using a light sensor E3S-C (Omron) with an External Trigger Reference Design Kit (QImaging). The

whole measuring process is controlled by an industrial computer, which is connected to the logistics of the factory. Controlling and analysis software is written in C++. Figure 6.6 shows the measuring setup and Figure 6.7 shows the developed user interface and the measuring view inside the system.

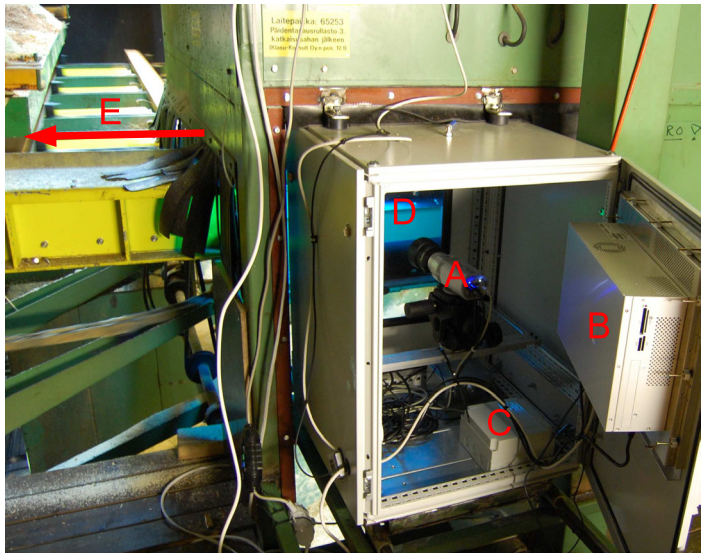

Figure 6.6: Developed measuring prototype. A is camera, B is industrial computer, C is control electronics and D is UV-light tubes and E is moving direction for the industrial line.

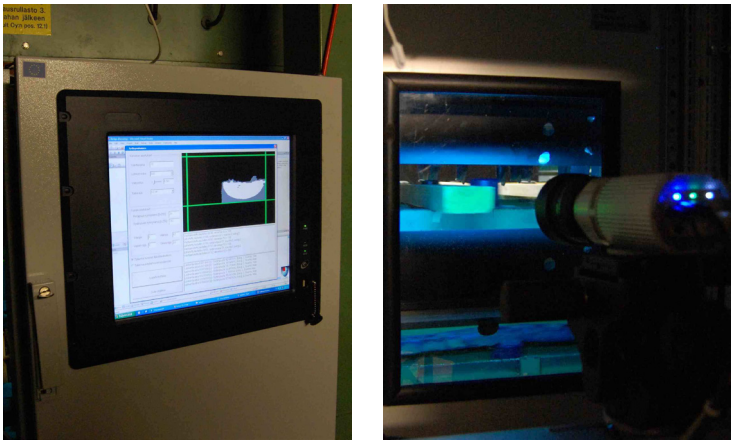

(a) (b)

Figure 6.7: (a) User interface for the measuring system. (b) Measuring view inside the rack.

6.3 SPECTRAL IMAGING IN NEUROSURGERY

The benefits of spectral imaging and spectroscopy in medical applications has been studied in several fields such as; tumor demarcation [18–20,90–92], the degeneration of cartilage [16], the early stage detection of the diabetes from retinal images [17], and so on.

The study of the identification of neoplastic tissues is important for improving the recovery process of a patient. In tumor resection, it is important to determine the tumor margins accurately, which is a difficult task. Ideally resection is made by removing the entire tumor without damaging the healthy tissue, but, as any tumorous tissue not removed can cause regrowth of the tumor, resection is usually made by removing some healthy tissue from around the tumor as well as a safety procedure.

Paper **P3** proposes an LCTF based spectral imaging system for a neurosurgical microscope. The microscope is used for neurosurgical operations such as brain surgeries and spine surgeries. Because the target operations have to be done accurately the spectral camera must not disturb the surgeon. If the spectral camera is too large, it may disturb the surgeon, or if the camera is too heavy the microscope cannot be stabilized. Therefore, a small, lightweight spectral camera is required. The spectral camera is constructed from a Varispec LCTF component [53], Basler monochrome camera and various optics. The measuring region for the system ranges from 420 to 720 nm. The LCTF component used provided a 10 nm spectral resolution, so the full resolution spectral image contains 31 wavelength channels. A connection setup for the spectral camera is shown in a Figure 6.8.

Figure 6.8: The spectral imaging system connected to Zeiss OPMI Pentero neurosurgery microscope. A *is the camera,* B *is the LCTF component,* C *is optics and* D *is the microscope.*

The spectral camera was tested in several different surgeries. It was used for collecting a database of different tissues. The collected tissue database can be used for future studies. Figure 6.9 shows an example of a human cortex and measured spectra.

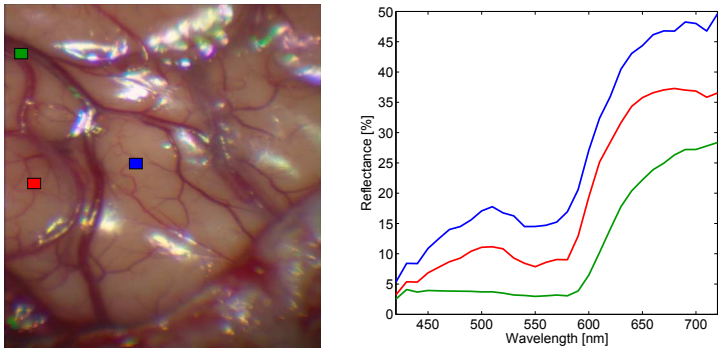

(a) (b)

Figure 6.9: (a) Converted RGB-image of a cortex. (b) Reflectance spectra from selected regions.

PCA was used for tissue separation in Paper **P3**. Use of PCA was studied to determine a margin between neoplastic and healthy tissue (Fig. 6.10). First three inner product images are shown in

Fig. 6.10(b–d). First and second inner product images can be used for good margin estimation between the healthy and neoplastic tissues. The test results for the tissue separation were based on a visual judgment of an expert. Thus, further studies with pathological reports are needed.

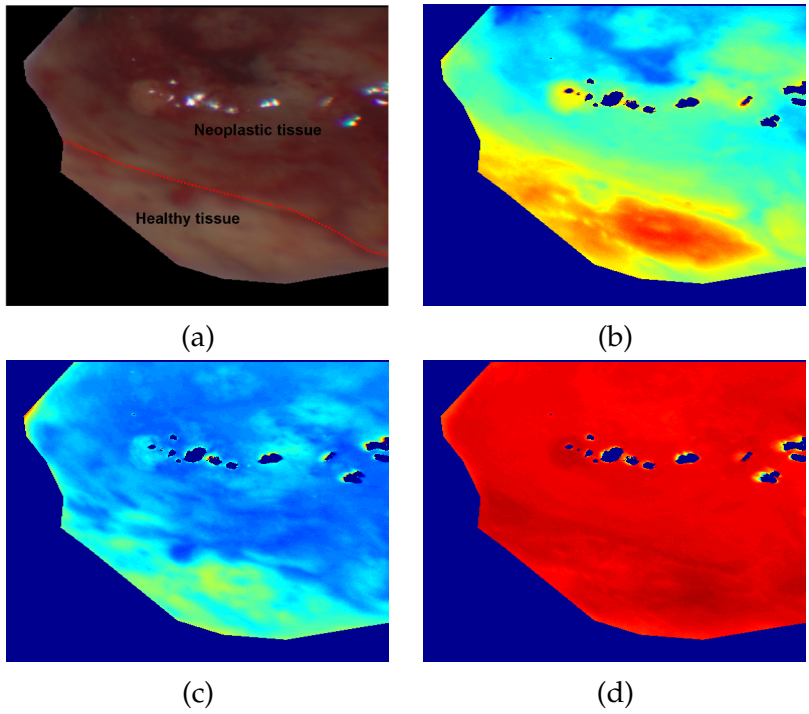

Figure 6.10: (a) Converted RGB-image of resected tumor tissue. First three inner product images (b) 1. inner product (c) 2. inner product and (d) 3. inner product.

6.4 COMPUTATIONAL TECHNIQUES

Two computational techniques for spectral image analysis were implemented and tested. The PCA computation was tested with several spectral images of different spatial and spectral resolutions. Figure 6.11 shows an example of a measured spectral image of a printed leaflet and the first six calculated eigenvectors. The first eigenvector is positive and it holds the mean data of the spectral image. It describes most of the variation inside the image. The second eigenvector produces the second largest variation of the image, and so on. Each eigenvector is uncorrelated and orthogonal to each other. Corresponding inner product images are shown in Figure 6.12. These inner product images and their combinations can be used for feature extraction. One example of PCA feature extraction was demonstrated in the previous section (Fig. 6.10). For future applications, it is necessary to increase the efficiency of the computation. Therefore, a faster implementation of the PCA is proposed and tested (Paper **P4**).

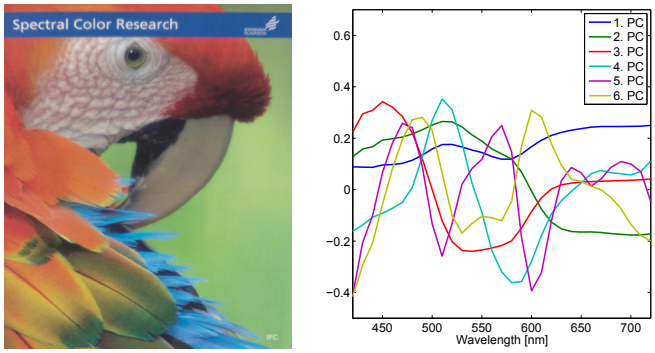

(a) (b)

Figure 6.11: (a) Converted RGB image from the spectral image. (b) First 6 principal components.

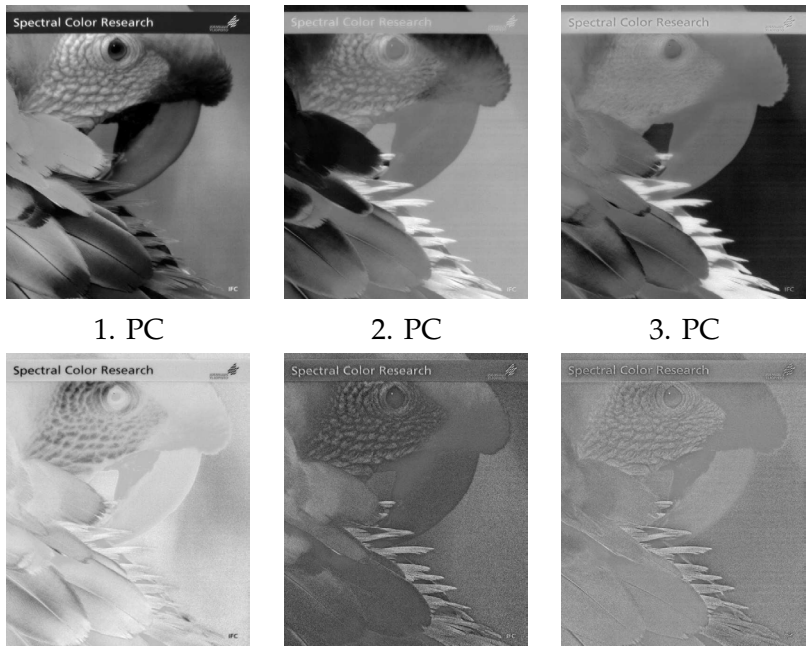

Figure 6.12: First 6 inner product images.

Computation of the PCA analysis was undertaken by use of a GPU (**P4**). The implementation was made in the NVIDIA CUDA programming environment [70]. The implementation was done in the C++ language using Microsoft Visual Studio. The PCA implementation was tested with two separate systems. Both of the systems contained Quad-core Xeon 3 GHz CPUs with 3 GB of DDR2 memory. One of the computers had an NVIDIA Quadro FX 3700 graphics card with 120 parallel processors with 512 MB of GDDR3 memory. The second computer was equipped with a GeForce GTX 280 graphics card with 240 parallel processors with 1 GB of GDDR3 memory. Comparison between the computation times of the graphics cards is not precise due the different main computers, but the results will give a good general view of the efficiency of the graphics cards.

Computation times were tested with square $N \times N$ spectral images with varying number of spectral channels. Different spectral images were generated from one spectral image by resizing the spatial domain and interpolating the spectral domain. Nevertheless, the computation time is related only to the actual size of the spectral data and not to the contents.

The GPU implementation increased the computational efficiency close to $7\times$ with the GTX 280 graphics card at the highest input size $N = 800$ (Fig. 6.13). Average differences between the computers and the graphics cards was around 35%. The computational efficiency did not rise significantly above the input size $N = 250$ in either of the setups. The copying time of the data from the CPU to GPU is relatively high compared with the total computation time.

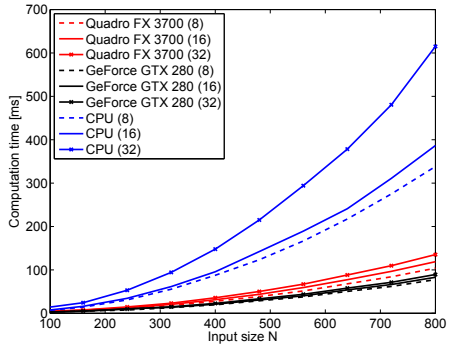

(a)

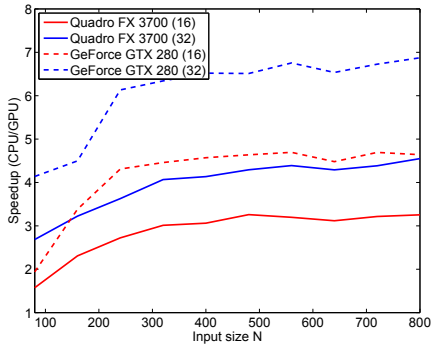

(b)

Figure 6.13: Computational times and speed-ups for the PCA calculation for spectral images with different spatial sizes and wavelength channels.

The second computational method tested was NTF. For spectral image analysis, this method can be used for compression, feature extraction and enhancing the color differences of the image. One of the applications of NTF is optimal filter calculation. Optimal filters can be used for enhancing the color differences in the image [93, 94]. Figure 6.14 shows one illustrative example where an arm was imaged from 420 to 720 nm in 10 nm steps. By using NTF, optimal filters for different features can be computed (Fig. 6.14b). After the original spectral image is filtered by the method presented in [93], discrimination between the blood vessels and the skin is increased (Fig. 6.14c).

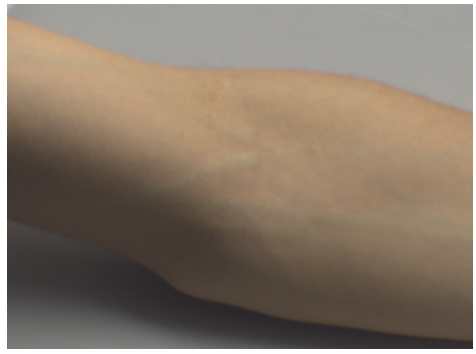

(a)

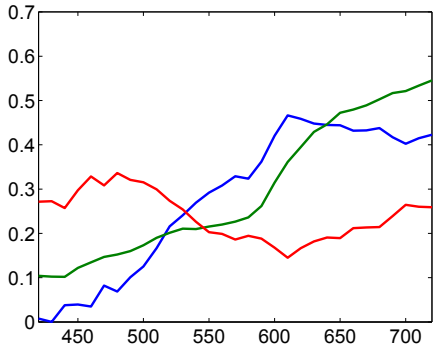

(b)

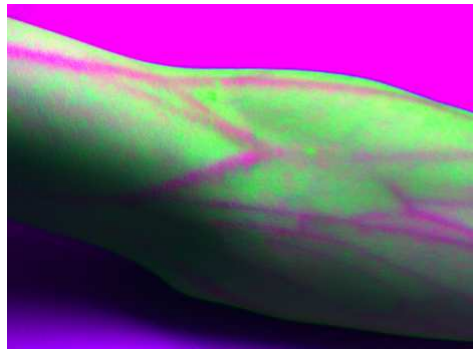

(c)

Figure 6.14: (a) Original RGB image from the spectral image. [93] (b) Calculated filters. c) Filtered RGB image.

The NTF computation of large data sets is normally very time-consuming and the computation time can rise from tens of minutes to hours. Some studies have proposed different methods to speed up the NTF computation [62,68], but the gained efficiencies of these implementations were not great. The Paper **P5** proposes a GPU implementation to speed up the computation process. Computational efficiency was tested for spectral images with different spatial sizes and different wavelength counts. Different spectral images for the testing were generated by resizing the spatial domain and interpolating the wavelength channels of one spectral image. Computation times were tested with fixed iterations, therefore the content of the data does not have any effect on the computational times.

The computer used for the tests contained an Intel i7-920 processor with 6 GB of DDR3 memory and an NVIDIA GeForce GTX280 graphics card with 1 GB of GDDR3 memory. Figure 6.15 shows computation times for NTF with 500 iterations calculated with the CPU (Fig. 6.15a) and the GPU (Fig. 6.15b). The speed-up factor (Fig. 6.15c) in the efficiency of the GPU implementation increased from 60$\times$ to 100$\times$. The result for the implementation efficiency is good and it significantly decreases the image analysis time from tens of minutes to seconds. This implementation provides faster applications for industry and for medical applications as well.

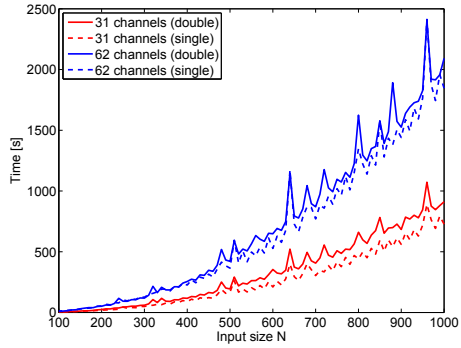

(a)

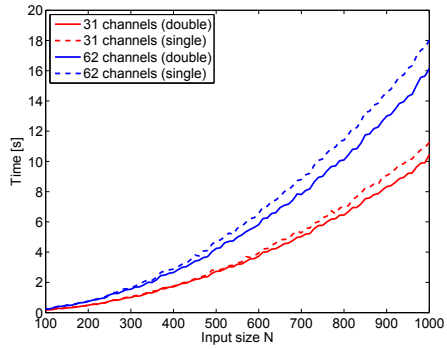

(b)

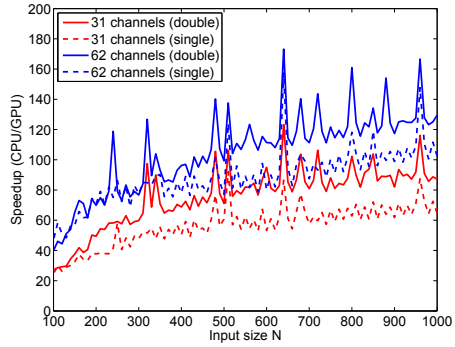

(c)

Figure 6.15: (a) Computational times for the NTF with different input sizes using the CPU. (b) Computational times for the NTF with different input sizes using the GPU. (c) Speedups for NTF calculation.

7 Discussion and conclusions

Selected spectral image acquisition techniques were analyzed for their benefits, weaknesses and prerequisites for industrial and medical applications. Three imaging systems were tested and proposed. The first was a line-scanning-based spectral imaging system with two spectral cameras. The proposed spectral imaging system has been used in several scientific projects and it has enabled measurement processes that were not possible before, especially in cases where the sample might be quickly contaminated. The developed system has been used for the determination of the moisture content of wooden boards.

Heartwood is an important feature and quality factor of wood. If the heartwood content can be detected, it may help to optimize the wood drying process. Heartwood contains less water than the sapwood; therefore, boards with a large amount of heartwood do not require as much drying time as boards with larger sapwood content. Information on the amount and the position of the heartwood in the logs can be used to determine optimal sawing parameters.

This thesis proposed a fluorescence imaging-based system for heartwood detection. Several studies related to heartwood detection using infrared imaging have been made [79, 80] with promising results. Infrared imaging can only be used for fresh and not for dried samples. Also, studies for heartwood detection using X-ray have been undertaken [78]. X-ray scanning is expensive and it is mainly used for logs. The proposed fluorescence method in this thesis can be used for both cases. Usage of the system can be easily expanded for log measurements. In addition, use of the fluorescence imaging method for classifying highly decay-resistant samples should be studied. Moreover, the cooperative company has applied for patents (Finnish Patent Application 20096322 [26], European Patent Application EP2345887 [25]), which are still under

review, for the fluorescence imaging method and the measuring prototype.

The usage of spectral imaging has expanded to the field of neurosurgery. The third spectral imaging system proposed was developed for a medical surgical microscope and the imaging was based on a small LCTF component. Previous studies [18, 19] have tested LCTF based cameras for brain tissue and tumor demarcation. However, the proposed system in this thesis is smaller and it can be used during surgery without disturbing the surgeon. This imaging system has been used *in vivo* for capturing 38 different spectral images during ten different surgical procedures. A spectral image database, from different biological tissues, has been collected and more is needed for future applications. Also, the imaging wavelength region should be increased to cover the near infrared region. In this study, the wavelength region was limited to the visible region, because the operation microscope used an infrared filter to block the infrared region due to the heat issue. The study of neurosurgical image capturing is progressing to real-time spectral imaging. Preliminary tests with tissue separation show good results but more comprehensive study is needed.

One main goal of this thesis was to increase the speed of the implementation of commonly used spectral image analysis algorithms. This thesis presented two implementations, the PCA and the NTF, through use of a GPU.

The implementation of the PCA did not produce such a marked benefit in the computational speed (about $7\times$). Most of the increase was achieved in the computation of the correlation matrix. Calculation of the eigen vectors and eigen values did not result in a remarkable increase. For a comparison, one parallel iterative PCA GPU implementation with about a $12\times$ increase in speed for high dimensional data has been introduced by M. Andercut [95]. The proposed approach in [95] is based on an iterative algorithm whereas this thesis proposes a non-iterative method. Iterative algorithms are mainly used for datasets that cannot be calculated through a correlation matrix, whereas the proposed method in this thesis assumes

that the correlation matrix can be calculated in the memory. Although the results between the iterative and non-iterative methods cannot be compared directly because of the different initial algorithms, nevertheless, the gained increase in speed for the PCA may enable some real-time analysis application, for example, fast tumor margin detection.

The GPU implementation of the NTF algorithm reduced the computational time remarkably ($60-100\times$) compared with the normal CPU implementation, depending on the size of the spectral image. For a comparison, only one parallel implementation for NTF was introduced by Zhang et al. [62]. They used a Sun Fire X4600 M2 server for the computation task and they reported around a $7\times$ increase in speed. At the time, no GPU implementations were available for the NTF computation.

The selection of the spectral camera is dependent on the target application. If the application is an industrial line, the line-scanning-based imaging system can be used. It is more suitable for monitoring tasks than a spectral based system. Spectral based systems are better for non-moving targets and especially for natural outdoor scenes where the line-scanning-based system cannot be so easily used.

Usually, spectral imaging is only needed in preliminary measurements. From these measurements, an application specific wavelength channel can be selected. These wavelength channels can be filtered and monitored with a monochrome camera. The proposed fluorescence imaging system is one good example of how the preliminary spectral measurements were used to select the correct illumination and the detection wavelength for the target features. Nevertheless, if the detection of the target features requires multiple wavelength channels, the use of a spectral camera is necessary.

Development of imaging systems should go forward. The main restriction in the field of application for spectral imaging systems is the speed. The imaging speed needs to be increased whilst keeping the spatial and spectral resolutions high. When the imaging times decrease, the analysis efficiency of the images must be improved.

For example, during brain surgery, the surgeon cannot wait several minutes between measurement and the production of the analyzed image. The resultant image should be displayed as quickly as possible. Therefore, a study of GPU implementations should be made in the future. Taking advantage of GPUs, in the sense of spectral image analysis, offers a huge potential for new applications, which have been postponed for years due to the restriction of slow computational times. Nowadays those problems might be solved in a reasonable time.

References

[1] R. S. Berns, *Billmeyer and Saltzman's principles of color technology* (New York: John Wiley & Sons, 2000).

[2] P. K. Kaiser and R. M. Boynton, *Human Color Vision* (Optical Society of America, 1996).

[3] W. A. Thornton, "How Strong Metamerism Disturbs Color Spaces," *Color research and application* 402–407 (1998).

[4] L. Harkonen, J. B. Martinkauppi, H. Laamanen, and M. H.-K. et al., "Spectral based optimization of screen images for industrial product presentation," in *Proc.* IS & T/SPIE's Electronic Imaging: Science and Technology, Vol. 6062 (2006).

[5] L. G. Coppel, M. Andersson, P. Edström, and J. Kinnunen, "Limitations in the efficiency of fluorescent whitening agents in uncoated paper," *Nordic Pulp & Paper Research Journal* 319–328 (2011).

[6] T. Rials, S. Kelley, and C.-L. So, "Use of Advanced Spectroscopic Techniques for Predicting the Mechanical Properties of Wood Composites," *Wood and Fiber Science* 398–407 (2002).

[7] D. Butler, C. Brunner, and J. Funck, "Wood-surface feature classification using extended-color information," *Holz als Roh- und Werkstoff* 475-482 (2001).

[8] P. Lebow, C. Brunner, A. Maristany, and D. Butler, "Classification of Wood Surface Features by Spectral Reflectance," *Wood and Fiber Science* 74–90 (1996).

[9] M. S. Kim, Y.-R. Chen, B.-K. Cho, K. Chao, C.-C. Yang, A. M. Lefcourt, and D. Chan, "Hyperspectral reflectance and fluorescence line-scan imaging for online defect and fecal contamina-

tion inspection of apples," *Sensing and Instrumentation for Food Quality and Safety* **1** (2007).

[10] J. Qiao, M. O. Ngadi, N. Wang, C. Gariépy, and S. Prasher, "Pork quality and marbling level assessment using a hyperspectral imaging system," *Journal of Food Engineering* **83,** 10 – 16 (2007).

[11] D. Barbin, G. Elmasry, D.-W. Sun, and P. Allen, "Near-infrared hyperspectral imaging for grading and classification of pork," *Meat Science* **90,** 259 – 268 (2012).

[12] T. Hyvarinen, E. Herrala, and A. Dall'Ava, "Direct sight imaging spectrograph: a unique add-on componet brings spectral imaging to industrial applications," in *Proc.* IS & T/SPIE's Symposium on Electronic Imaging: Science and Technology *(EI98)*, Vol. 3302-21 (1998).

[13] K. Nishino, M. Nakamura, M. Matsumoto, O. Tanno, and S. Nakauchi, "Imaging of Cosmetics Foundation Distribution by a Spectra Difference Enhancement Filter," in *Proceedings of the 5th European Conference on Colour in Graphics, Imaging, and Vision, CGIV* (2010), pp. 275–281.

[14] D. Jia and T. Ding, "Detection of foreign fibers in cotton using near-infrared optimal wavelength imaging," *Optical Engineering* **44,** 076402 (2005).

[15] T. Yotsuda, T. Yamamoto, H. Ishizawa, T. Nishimatsu, and E. Toba, "Near infrared spectral imaging for water absorbency of woven fabrics," in *Instrumentation and Measurement Technology Conference, 2004. IMTC 04. Proceedings of the 21st IEEE*, Vol. 3 (2004), pp. 2258–2261.

[16] J. Kinnunen, J. S. Jurvelin, J. Mäkitalo, M. Hauta-Kasari, P. Vahimaa, and S. Saarakkala, "Optical spectral imaging of degeneration of articular cartilage," *Journal of Biomedical Optics* **15,** 046024 (2010).

[17] P. Fält, J. Hiltunen, M. Hauta-Kasari, I. Sorri, V. Kalesnykiene, and H. Uusitalo, "Extending Diabetic Retinopathy Imaging from Color to Spectra," in *Image Analysis*, Vol. 5575, Lecture Notes in Computer Science (2009), pp. 149–158.

[18] S. C. Gebhart, *Liquid-Crystal Tunable Filter Spectral Imaging fort Discrimination Between Normal and Neoplastic Tissues In the Brain*, PhD thesis (Vanderbilt University, 2006).

[19] S. C. Gebhart, R. C. Thompson, and A. Mahadevan-Jansen, "Liquid-crystal tunable filter spectral imaging for brain tumor demarcation," *Appl. Opt.* **46,** 1896–1910 (2007).

[20] S. A. Toms, W.-C. Lin, R. J. Weil, M. D. Johnson, E. D. Jansen, and A. Mahadevan-Jansen, "Intraoperative optical spectroscopy identifies infiltrating glioma margins with high sensitivity," *Neurosurgery* (2005).

[21] I. Kuzmina, I. Diebele, D. Jakovels, J. Spigulis, L. Valeine, J. Kapostinsh, and A. Berzina, "Towards noncontact skin melanoma selection by multispectral imaging analysis," *Journal of Biomedical Optics* (2011).

[22] H. Akbari, Y. Kosugi, K. Kojima, and N. Tanaka, "Blood vessel detection and artery-vein differentiation using hyperspectral imaging," in *Engineering in Medicine and Biology Society, 2009. EMBC 2009. Annual International Conference of the IEEE* (2009), pp. 1461 –1464.

[23] M. Hauta-Kasari, J. Antikainen, M. Regmi, M. Kaemba, T. Jääskeläinen, and J. Parkkinen, "Spectral Image Acquisition of Icons," in *Proceedings of the 5th IS&T's Archiving Conference (Archiving 2008)* (2008), pp. 150–154.

[24] R. S. Berns and F. H. Imai, "The use of multi-channel visible spectrum imaging for pigment identification," in *13TH Triennial Meeting Rio de Janeiro Preprints, ICOM Committee for Conservation* (2002), pp. 217–222.

[25] S. Hämäläinen, P. Hyvönen, J. Antikainen, and J. Kinnunen, "Process and apparatus for determining the properties of a piece of timber," (2011), Patent EP2345887.

[26] S. Hämäläinen, P. Hyvönen, J. Antikainen, and J. Kinnunen, "Menetelmä ja laitteisto sahatavarakappaleen ominaisuuksien määrittämiseksi," (2011), Patent 20096322.

[27] R. Hunt, *Measuring Colour* (Fountain Press, England, 1998).

[28] G. Wyszecki and W. S. Stiles, *Color Science: Concepts and Methods, Quantitative Data and Formulae, 2nd edition* (Wiley-Interscience, 2000).

[29] J. A. Curcio and C. C. Petty, "The Near Infrared Absorption Spectrum of Liquid Water," *J. Opt. Soc. Am.* **41,** 302–302 (1951).

[30] J. Lehtonen, *Spectral Sampling and Spectral Image Compression*, PhD thesis (University of Joensuu, 2009).

[31] T. I. O. for Standardization, "Space environment (natural and artificial) Process for determining solar irradiances," (2007).

[32] B. D. Jordan and M. A. OŠNeill, "The whiteness of paper - colorimetry and visual ranking," *TAPPI* (1991).

[33] L. Coppel, M. Andersson, and P. Edström, "Determination of quantum efficiency of flourescing turbid media," *Applied Optics* (2011).

[34] R. Donaldson, "Spectrophotometry of fluorescent pigments," *British Journal of Applied Physics* **5,** 210 (1954).

[35] E. B. Bayer, "Color imaging array," U.S. Patent No. 3,971,065 (1976).

[36] Sony, "Press Releases - Realization of natural color reproduction in Digital Still Cameras, closer to the natural sight perception of the human eye," (2003).

[37] O. Kenro, A. Takeyuki, K. Yasuhiro, F. Hiroyuki, H. Hideaki, Y. Masahiro, and O. Nagaaki, "Six band HDTV camera system for spectrum-based color reproduction," *The Journal of Imaging Science and Technology* 85–92 (2004).

[38] F. Incorporated, "FD-1665 3-CCD Multispectral Camera," (2011), http://www.fluxdata.com.

[39] T. Jetsu, P. Hertzog, T. Jääskeläinen, and J. Parkkinen, "Standardization of Spectral Image Formats," *Pattern Recognition and Image Analysis* **15,** 618–620 (2005).

[40] M. Hauta-Kasari, J. Lehtonen, J. Parkkinen, and T. Jääskeläinen, "Image Format for Spectral Image Browsing," IS & T Journal of Imaging Science and Technology **50** (2006).

[41] F. S. Jon Y. Hardeberg and H. Brettel, "Multispectral color image capture using a liquid crystal tunable filter," *Optical Engineering* **41** (2002).

[42] W. R. Johnson, D. W. Wilson, W. Fink, M. Humayun, and G. Bearman, "Snapshot hyperspectral imaging in ophthalmology," *Journal of Biomedical Optics* (2007).

[43] "Specim's Web page," Specim, online (2012), http://www.specim.fi, last accessed March 2012.

[44] J. Antikainen, M. Hauta-Kasari, J. Parkkinen, and T. Jääskeläinen, "Automated Spectral Image Measurement Software," in *Proceedings of the 9th International Symposium on Multispectral Colour Science and Application (MCS07)* (2007), pp. 195–200.

[45] N. Gat, "Imaging Spectroscopy Using Tunable Filters: A Review," in *Proc.* SPIE–The International Society for Optical Engineering, Vol. 4056 (2000), pp. 50–64.

[46] K. Itoh, "Interferometric multispectral imaging," Progress in Optics XXXV *(E. Wolf, ed)* 145–196 (1996).

[47] S. J. Woltman, G. D. Jay, and G. P. Crawford, "Liquid-crystal materials find a new order in biomedical applications," *Nature Materials* (2007).

[48] C. Sobrinhoa, J. Limab, E. de Almeidab, and A. Sombrab, "Acousto-optic tunable filter (AOTF) with increasing non-linearity and loss," *Optics Communications* **208,** 415–426 (2002).

[49] K. Itoh, T. Inoue, T. Yoshida, and Y. Ichioka, "Interferometric supermultispectral imaging," *Applied Optics* **29** (1990).

[50] L. Gao, R. T. Smith, and T. S. Tkaczyk, "Snapshot hyperspectral retinal camera with the Image Mapping Spectrometer (IMS)," *Biomed. Opt. Express* **3,** 48–54 (2012).

[51] K. A. Bakeev, *Process Analytical Technology: Spectroscopic Tools and Implementation Strategies for the Chemical and Pharmaceutical Industries, 2nd Edition* (John Wiley & Sons, Ltd., 2010).

[52] "Edmund Optics Web page," Edmund Optics, online (2012).

[53] I. Cambridge Research & Instrumentation, "TECHNICAL NOTE: FAQs & Principles of Operation, VariSpec Liquid Crystal Tunable Filters," (2010).

[54] D. Dussaulta and P. Hoess, "Noise performance comparison of ICCD with CCD and EMCCDcameras," in *Proceedings of SPIE*, Vol. 5563 (2004), pp. 195–204.

[55] I. Jolliffe, *Principal Component Analysis, Second Edition* (Springer, 2002).

[56] J. Lehtonen, J. Parkkinen, and T. Jääskeläinen, "Optimal Sampling of Color Spectra," *Journal of Optical Society of America A* 2983–2988 (2006).

[57] T. Jääskeläinen, R. Silvennoinen, J. Hiltunen, and J. P. S. Parkkinen, "Classification of the reflectance spectra of pine, spruce, and birch," *Appl. Opt.* **33,** 2356–2362 (1994).

[58] A. Andriyashin, J. Parkkinen, and T. Jääskeläinen, "Illuminant dependence of PCA, NMF and NTF in spectral color imaging," in *19th International Conference on Pattern Recognition (ICPR 2008), December 8-11, 2008, Tampa, Florida, USA* (2008), pp. 1–4.

[59] R. Jošth, J. Antikainen, J. Havel, A. Herout, P. Zemčík, and M. Hauta-Kasari, "Real-time PCA calculation for spectral imaging (using SIMD and GP-GPU)," *Journal of Real-Time Image Processing* 1-9 (2011).

[60] J. P. S. Parkkinen, J. Hallikainen, and T. Jääskeläinen, "Characteristic spectra of Munsell colors," *J. Opt. Soc. Am. A* **6,** 318–322 (1989).

[61] R. Lenz and T. H. Bui, "Statistical properties of color-signal spaces," *Journal of Optical Society of America* **22,** 820–827 (2005).

[62] Q. Zhang, M. W. Berry, B. T. Lamb, and T. Samuel, *A Parallel Nonnegative Tensor Factorization Algorithm for Mining Global Climate Data*, Vol. 5545, (Springer Berlin / Heidelberg, 2009), pp. 405–415.

[63] A. H. Andersen and W. S. Rayens, "Structure-seeking multilinear methods for the analysis of fMRI data," *NeuroImage* **22,** 728–739 (2004).

[64] T. G. Kolda and B. W. Bader, "Tensor Decompositions and Applications," *SIAM Review* 455-500 (2009).

[65] D. FitzGerald, M. Cranitch, and E. Coyle, "Non-Negative Tensor Factorisation for Sound Source Separation," in *Proceedings of Irish Signal and Systems Conference* (2005).

[66] M. Kim and S. Choi, "Monaural Music Source Separation: Nonnegativity, Sparseness, and Shift-Invariance," in *6th international conference on Independent Component Analysis and Blind Signal Separation* (2006), pp. 617–624.

[67] T. Hazan, S. Polak, and A. Shashua, "Sparse image coding using a 3D non-negative tensor factorization," in *Proc. Tenth IEEE International Conference on Computer Vision (ICCV 2005)*, Vol. 1 (2005), pp. 50–57.

[68] A. Kaarna, A. Andriyashin, S. Nakauchi, and J. Parkkinen, *Multiresolution Approach in Computing NTF*, Vol. 4522, (Springer Berlin / Heidelberg, 2007), pp. 334–343.

[69] L. Grippo and M. Sciandrone, "On the convergence of the block nonlinear Gauss-Seidel method under convex constraints," *Operations Research Letters* **26,** 127–136 (2000).

[70] NVIDIA, *NVIDIA CUDA Programming Guide 3.0* (NVidia, 2010).

[71] P. Arbenz, "Lecture Notes on Solving Large Scale Eigenvalue Problems," (2010).

[72] O. Hagman, *On Reflections of Wood*, PhD thesis (Luleå University of Technology, Sweden, 1996).

[73] H. Kauppinen, *Development of a Color Machine Vision Method for Wood Surface Inspection*, PhD thesis (University of Oulu, Finland, 1999).

[74] J. Lampinen, S. Smolander, and M. Korhonen, *Wood Surface Inspection System Based on Generic Visual Feature* (Industrial Applications of Neural Networks, World Scientific Publishing, Singapore, 1998), pp. 35–42.

[75] D. E. Kline, C. Surak, and P. Araman, "Automated Hardwood Lumber Grading Utilizing a Multiple Sensor Machine Vision Technology," *Computers and Electronics in Agriculture* 139–155 (2003).

[76] B. G. Batchelor and P. F. Whelan, *Intelligent Vision Systems for Industry* (Springer, 1997).

[77] P. Österberg, *Wood Quality and Geometry Measurements Based on Cross Section Images*, PhD thesis (Tampere University of Technology, 2009).

[78] S. Johan and O. Johan, "Heartwood diameter measurements in Pinus sylvestris sawlogs combining X-ray and three-dimensional scanning," *Scandinavian Journal of Forest Research* (2009).

[79] F. Arnerup, "Infrared Imaging of Scots Pine Cross Sections: Automatic Heartwood Size Measurements," Master of Science thesis (2002).

[80] P. Gjerdrum and O. Hoibo, "Heartwood detection in Scots pine by means of heat-sensitive infrared images," *Holzforschung* 131–136 (2004).

[81] P. Kärenlampi and M. Riekkinen, "Prediction of the heartwood content of pine logs," *Wood and Fiber Science* (2003).

[82] I. Johansson, "Förfarande för kvalitetsbestämning av trämaterial," Patent SE520447 (2003).

[83] H. Hovelstad, I. Leirset, K. Oyaas, and A. Fiksdahl, "Screening analyses of pinosylvin stilbenes, resin acids and lignans in Norwegian conifers," *Molecules* 103–114 (2006).

[84] S. Willför, J. Hemming, M. Reunanen, and B. Holmbom, "Phenolic and Lipophilic Extractives in Scots Pine Knots and Stemwood," *Holzforschung* 359–372 (2003).

[85] O. Karppanen, M. Venäläinen, A. M. Harju, S. Willför, S. Pietarinen, T. Laakso, and P. Kainulainen, "Knotwood as a window to the indirect measurement of the decay resistance of Scots pine heartwood," *Holzforschung* 600–604 (2007).

[86] C. Celimene, J. Micales, L. Ferge, and R. Young, "Efficacy of Pinosylvins Against White–Rot and Brown–Rot Fungi," *Holzforschung* 491–497 (1999).

[87] M. Venäläinen, A. Harju, P. Kainulainen, H. Viitanen, and H. Nikulainen, "Variation in the Decay Resistance and its Relationship With Other Wood Characteristics in Old Scots Pines," *Annals of Forest Science* 409–417 (2003).

[88] H. Erdtman and E. Rennerfelt, "The pinosylvin-phenolic content of pine heartwood; its determination and its antiseptic action towards wood-destroying fungi," *Svensk Papper* 45–56 (1944).

[89] J. Hart and D. M. Shrimpton, "Role of Stilbenes in Resistance of Wood to Decay," *Phytopathology* 1138–1143 (1979).

[90] W. Mier, B. Beijer, K. Graham, and W. E. Hull, "Fluorescent Somatostatin Receptor Probes for the Intraoperative Detection of Tumor Tissue with Long-Wavelength Visible Light," *Bioorganic & Medicinal Chemistry* **10,** 2543 – 2552 (2002).

[91] Y. Kajimoto, S.-I. Miyatake, and T. Kuroiwa, "Fiber-optic spectroscopic detection of neoplasm by intraoperative fluorescence labeling," *International Congress Series* **1259,** 33 – 38 (2004), Developments in Neuroscience. Proceedings of the 3rd International Mt. Bandai Symposium for Neuroscience and the 4th Pan-Pacific Neurosurgery Congress.

[92] R. Andreas, B. Jörgen, G. Rödiger, Z. Michael, and S. Volker, "Near-infrared Indocyanine Green Video Angiography: A New Method for Intraoperative Assessment of Vascular Flow," *Neurosurgery* **52,** 132–139 (2003).

[93] A. Kaarna, K. Nishino, K. Miyazawa, and S. Nakauchi, "Michromatic scope for enhancement of color difference," *Color Research & Application* **35,** 101–109 (2010).

[94] K. Nishino, A. Kaarna, K. Miyazawa, H. Oda, and S. Nakauchi, "Optical implementation of spectral filtering for the enhancement of skin color discrimination," *Color Research & Application* 53–58 (2010).

[95] M. Andrecut, "Parallel GPU Implementation of Iterative PCA Algorithms," *Journal of Computational Biology* **16,** 1593–1599 (2009).

Jukka Antikainen

New Techniques for Spectral Image Acquisition and Analysis

The objective of this thesis was to study new spectral image acquisition techniques and analysis methods. Three different imaging systems were developed and tested. This thesis proposed the implementation of two statistical methods for spectral image analysis. Implementations were done using Graphical Processing Units (GPUs) and computational speed-up of the analyzing algorithms was compared against ordinary (non-GPU) implementations. The imaging systems and software implementations have been used in research projects that are presented as case studies in the thesis.

UNIVERSITY OF
EASTERN FINLAND

Publications of the University of Eastern Finland
Dissertations in Forestry and Natural Sciences

ISBN: 978-952-61-0817-9 (printed)
ISSNL: 1798-5668
ISSN: 1798-5668
ISBN: 978-952-61-0818-6(pdf)
ISSNL: 1798-5668
ISSN: 1798-5676